JGR Solid Earth

RESEARCH ARTICLE
10.1029/2019JB018289

A Joint Analysis of GPS Displacement and GRACE Geopotential Data for Simultaneous Estimation of Geocenter Motion and Gravitational Field

Mahdiyeh Razeghi[1], Shin-Chan Han[1], Simon McClusky[2], and Jeanne Sauber[3]

[1]School of Engineering, University of Newcastle, Callaghan, New South Wales, Australia, [2]Research School of Earth Sciences, Australian National University, Canberra, ACT, Australia, [3]Geodesy and Geophysics Laboratory, NASA Goddard Space Flight Center, Greenbelt, MD, USA

Key Points:
- The study shows a technique for simultaneous estimation of geocenter motion and gravitational potential field by a GPS/GRACE joint inversion
- The results of geocenter motion (degree one) are most consistent with the Satellite Laser Ranging results
- Dense GPS data contributed to higher-degree coefficients of gravity fields and improved water storage in major US and European river basins

Correspondence to:
M. Razeghi,
seyedehmahdiyeh.razeghi@uon.edu.au

Citation:
Razeghi, M., Han, S.-C., McClusky, S., & Sauber, J. (2019). A joint analysis of GPS displacement and GRACE geopotential data for simultaneous estimation of geocenter motion and gravitational field. *Journal of Geophysical Research: Solid Earth*, *124*. https://doi.org/10.1029/2019JB018289

Received 29 JUN 2019
Accepted 1 OCT 2019
Accepted article online 22 OCT 2019

Abstract Gravitational potential data from GRACE are being used to study mass redistribution within and between the atmosphere, hydrosphere, cryosphere, and solid Earth. The GRACE data are made available in a reference frame with its origin at the center of mass of the Earth system (geocenter) while many other geophysical models and data sets refer to a reference frame attached to the Earth's surface. Changes in the offset between these reference frames (geocenter motion) must be accounted for when GRACE data are used to quantify surface mass changes. In this study, we developed a technique for co-estimation of geocenter motion and gravitational potential field seamlessly from degree 1 to 90 by simultaneously inverting a set of globally-distributed GPS displacement time series and the temporally-varying GRACE gravity data. We found that the effect of geocenter motion was evident particularly in the GPS time series of horizontal displacements. Our estimates of geocenter motion are most consistent with the Satellite Laser Ranging (SLR) results within 1 mm in X and Z components and a submillimeter in Y component, when compared to monthly variability averaged over the period of 2003–2016. The overall magnitude of the degree-1 ($l = 1$) surface mass load is estimated to be ~3 cm in equivalent water height annually migrating south-westward from Europe (December–January) to the South Pacific (June–July). Our results also show that dense GPS network data improve water storage recovery in major river basins in the United States and Europe by contributing significantly to the recovery of higher-degree ($l \geq$ ~20) geopotential coefficients.

1. Introduction

Global geopotential fields have been measured by Gravity Recovery And Climate Experiment (GRACE) approximately monthly between August 2002 and June 2017 and by the GRACE Follow-On satellite mission starting June 2018 (Tapley et al., 2004; Webb et al., 2018). They are used to infer surface mass redistribution of water, air, snow, and ice after removing the effect of solid Earth's load deformation from the observed geopotential fields (Tapley et al., 2019; Wahr et al., 1998). Such geopotential measurements (Level-2 data products) are derived primarily from inter-satellite tracking data between two GRACE satellites orbiting around the instantaneous center of mass (CM) of the Earth system (Bettadpur, 2012). The origin of the reference frame used for monthly GRACE geopotential measurements is a quasi-instantaneous (monthly) CM, defined by setting the degree-1 geopotential (Stokes) coefficients to be zero. This introduces a difficulty in the application of GRACE data to study surface mass redistribution because other geophysical data and models are made available in a reference frame tied to the shape of the Earth's surface or its center of figure (CF) (not mass).

Over the last several decades, accurate surface deformation measurements have been made utilizing the Global Positioning System (GPS). More recently, lower-cost GPS ground receiver hardware and improvements in global communication infrastructure have led to an explosion in the availability of continuous global observations. Continuous daily GPS observations from thousands of stations are currently routinely collected and processed using highly efficient Precise Point Positioning (PPP) methods (Blewitt et al., 2018). Theses temporally dense, and increasingly spatially dense, daily global time-series capture the complete three-dimensional (3D) deformation of the Earth's surface reflecting, among other geophysical processes, the solid (elastic) Earth's response under surface mass loading (Farrell, 1972). Independently from GRACE, GPS displacement data in previous studies have been used to recover surface mass changes globally

(e.g., Blewitt & Clarke, 2003; Kusche & Schrama, 2005) and regionally (e.g., Argus et al., 2017; Borsa et al., 2014; Fu et al., 2015; Han & Razeghi, 2017). The GPS geocentric position vectors are usually referenced to International Terrestrial Reference Frame (ITRF) which has its origin coincident with the long-term mean CM (Altamimi et al., 2016). Therefore, the surface mass changes determined from GPS displacements and GRACE geopotential fields use a potentially inconsistent reference frame.

The relative motions of CM with respect to ITRF origin (i.e., geocenter motion) are found by computing the first moment of global mass distribution and are thus directly related to the degree-1 coefficients of geopotential and/or surface mass load defined in ITRF (Jekeli, 2015). They can be determined by different techniques; a comprehensive review on geocenter motion is available by Wu et al. (2012) and numerous papers cited therein. Here, we only name three distinct studies of direct relevance to this paper, including the solutions obtained by the analysis of satellite laser ranging (SLR) data from multiple geodetic satellites (Cheng et al., 2013), the determination of degree-1 load mass from GRACE data and ocean bottom pressure (OBP) model outputs (Swenson et al., 2008), and the global inversion of GPS, GRACE, and OBP data (Wu et al., 2010). These solutions of degree-1 components can be added to GRACE's higher-degree estimates of surface mass changes.

Extending the "degree-1 deformation" approach after Blewitt et al. (2001) and Lavallée et al. (2006), Han (2016) found coherent deformation of the entire Australian continent after removing the higher-degree deformation using GRACE from GPS measurements; the continent concurrently and seasonally shifts back and forth in a northwest-southeast axis by a couple of mm. Indeed, such degree-1 load deformation is the second largest horizontal displacement after the tectonic plate motion (~7 cm/year) in Australia. This study also showed that it is possible to estimate the seasonal geocenter motion and the degree-1 coefficients of surface mass from continental-scale movement. The work of Chanard et al. (2018) also determined the estimates of degree-1 coefficients from GRACE and global GPS data, and demonstrated improved comparison of the computed displacements from their degree-1 solutions with GPS measurements (particularly the horizontal components).

In this study, we develop a methodology to invert global GPS position time series and GRACE geopotential measurements simultaneously to determine the geopotential fields seamlessly from degree 1 to 90 solutions. These geopotential fields can be readily used to infer global surface mass changes in a reference frame (like ITRF) compatible with other geophysical data and models. We also show that our new geopotential solutions are improved significantly in regions with the most dense GPS network coverage. We describe in detail how we combine the two distinct data sets propagating their respective statistical information. The joint geopotential solutions are assessed for degree-1 coefficients only and higher-degree components by comparing with other solutions of geocenter motion and evaluating basin average water storage changes. Finally, we highlight the importance of geocenter motion in computation of terrestrial water storage changes in arid and semi-arid regions.

2. Method

In this section, we develop a joint analysis of GPS and GRACE data based on an elastic loading model (Farrell, 1972), assuming that the GPS surface deformation and GRACE geoid change are the result of the elastic Earth deformation caused by surficial mass load. However, as pointed out by Chao (2016), there are contributions by non-surficial processes to GRACE time-variable gravity measurements such as tidal forces, glacial isostatic adjustment (GIA), earthquakes, and plate tectonic processes which effect surface deformation and geopotential fields. In particular, Chambers et al. (2010) demonstrated the importance of the GIA correction and model uncertainty in evaluating ocean mass from GRACE. Section 3 describes how we accounted for such non-surficial effects in GPS and GRACE data sets before we combine them into solutions of global surface mass changes.

2.1. Observation Equations of Surface Displacement and Geopotential Changes

We consider a mass load $\sigma(\theta, \lambda, t)$ imposed on the Earth's surface (θ, λ) at time t, for example, mass redistribution caused by the atmosphere, ocean, and terrestrial water storage. It is represented in terms of equivalent water height and is expanded using a series of surface spherical harmonic functions:

$$\sigma(\theta,\lambda,t) = a\sum_{l=1}^{\infty}\sum_{m=0}^{l}\left\{C_{lm}^{\sigma}\{t\}\cos m\lambda + S_{lm}^{\sigma}\{t\}\sin m\lambda\right\}\overline{P}_{lm}(\cos\theta), \tag{1}$$

where $C_{lm}^{\sigma}(t)$ and $S_{lm}^{\sigma}(t)$ are the (dimensionless) coefficients of the load at degree l and order m, and a is the mean radius of the spherical Earth. $\overline{P}_{lm}$ is the associated Legendre function following normalization after Heiskanen and Moritz (1967). Conservation of global mass constrains the degree zero coefficient to be zero (i.e., $C_{00} = 0$).

The elastic Earth immediately responds to the surface load such that the Earth's surface deforms by $e(\theta,\lambda,t)$, $n(\theta,\lambda,t)$ and $u(\theta,\lambda,t)$ in east, north, and up components, respectively, and the geoidal (physical) surface changes due to attraction by the load and the underlying solid Earth deformation by $g(\theta,\lambda,t)$. Expressing the deformation and the geoidal surface change in terms of spherical harmonic series, we have

$$e(\theta,\lambda,t) = a\sum_{l=1}^{\infty}\frac{l_l^{'}}{1+k_l^{'}}\sum_{m=0}^{l} m\left\{-\overline{C}_{lm}(t)\sin m\lambda + \overline{S}_{lm}(t)\cos m\lambda\right\}\frac{\overline{P}_{lm}(\cos\theta)}{\sin\theta}, \tag{2}$$

$$n(\theta,\lambda,t) = a\sum_{l=1}^{\infty}\frac{l_l^{'}}{1+k_l^{'}}\sum_{m=0}^{l}\left\{-\overline{C}_{lm}(t)\cos m\lambda - \overline{S}_{lm}(t)\sin m\lambda\right\}\frac{\partial\overline{P}_{lm}(\cos\theta)}{\partial\theta}, \tag{3}$$

$$u(\theta,\lambda,t) = a\sum_{l=1}^{\infty}\frac{h_l^{'}}{1+k_l^{'}}\sum_{m=0}^{l}\left\{\overline{C}_{lm}(t)\cos m\lambda + \overline{S}_{lm}(t)\sin m\lambda\right\}\overline{P}_{lm}(\cos\theta), \tag{4}$$

$$g(\theta,\lambda,t) = a\sum_{l=1}^{\infty}\sum_{m=0}^{l}\left\{\overline{C}_{lm}(t)\cos m\lambda + \overline{S}_{lm}(t)\sin m\lambda\right\}\overline{P}_{lm}(\cos\theta), \tag{5}$$

where $h_l^{'}, l_l^{'}$, and $k_l^{'}$ are the load Love numbers of vertical, horizontal displacement, and gravitational potential, respectively. The coefficients $\overline{C}_{lm}(t)$ and $\overline{S}_{lm}(t)$ in the brackets are (dimensionless) coefficients of the geopotential changes (Farrell, 1972). They are related to the surface mass load coefficients through $\overline{C}_{lm}(t) = \frac{3\rho_w}{\rho_e}\frac{1+k_l^{'}}{2l+1}C_{lm}^{\sigma}(t)$ and $\overline{S}_{lm}(t) = \frac{3\rho_w}{\rho_e}\frac{1+k_l^{'}}{2l+1}S_{lm}^{\sigma}(t)$ with the density of surface mass load (in terms of water), $\rho_w = 1{,}000\ \mathrm{kg/m^3}$, and the average density of the elastic Earth, $\rho_e = 5{,}517\ \mathrm{kg/m^3}$. The factor $1 + k_l^{'}$ accounts for the direct effect of surface mass and the indirect effect caused by elastic adjustment of the Earth to the surface mass (Wahr et al., 1998).

The degree-1 geopotential coefficients are related to the first moment of mass distribution within the Earth (Jekeli, 2015). In this study, we assume the mass redistribution $\sigma(\theta,\lambda,t)$ only on the Earth's surface. The coordinates of the center of mass redistribution can be found by computing global integration of $\sigma(\theta,\lambda,t)$ multiplied by its location over the Earth's sphere as follows:

$$X_{CM}(t) = \sqrt{3}a\overline{C}_{1,1}(t), \tag{6a}$$

$$Y_{CM}(t) = \sqrt{3}a\overline{S}_{1,1}(t), \tag{6b}$$

$$Z_{CM}(t) = \sqrt{3}a\overline{C}_{1,0}(t), \tag{6c}$$

where $X_{CM}(t)$, $Y_{CM}(t)$, and $Z_{CM}(t)$ are the time-variable Cartesian coordinates indicating the instantaneous center of mass (CM) with respect to the origin of the reference frame used to define $\sigma(\theta,\lambda,t)$ in equation (1).

The GRACE satellites, like all others, are orbiting around the CM of the Earth system, which renders the GRACE inter-satellite tracking data insensitive to the degree-1 geopotential coefficients (or geocenter motion) in equation (6). The GRACE data include monthly time series of coefficients $\overline{C}_{lm}(t)$ and $\overline{S}_{lm}(t)$ only for $l \geq 2$ and $m \geq 0$ in equation (5). In contrast, GPS displacement data, when signals not associated with elastic load deformation (like tectonic motion) are removed, may infer all $\overline{C}_{lm}(t)$ and $\overline{S}_{lm}(t)$ including the degree-1 coefficients that pinpoint the locations of CM from the origin of a reference frame of the GPS data used.

In the following equations, we define the degree-1 displacement as the elastic deformation contributed only by the degree-1 geopotential coefficients (or the degree-1 surface mass load):

$$e_1(\theta,\lambda,t) = a\frac{\sqrt{3}l_1^{'}}{1+k_1^{'}}\{-\overline{C}_{1,1}(t)\sin\lambda + \overline{S}_{1,1}(t)\cos\lambda\}, \tag{7}$$

$$n_1(\theta,\lambda,t) = a\frac{\sqrt{3}l_1^{'}}{1+k_1^{'}}\{\overline{C}_{1,0}(t)\sin\theta - \overline{C}_{1,1}(t)\cos\theta\cos\lambda - \overline{S}_{1,1}(t)\cos\theta\sin\lambda\}, \tag{8}$$

$$u_1(\theta,\lambda,t) = a\frac{\sqrt{3}h_1^{'}}{1+k_1^{'}}\{\overline{C}_{1,0}(t)\cos\theta + \overline{C}_{1,1}(t)\sin\theta\cos\lambda + \overline{S}_{1,1}(t)\sin\theta\sin\lambda\}. \tag{9}$$

Han (2016) used GRACE data to compute the load displacements for $l \geq 2$ and subtracted them from GPS data to compute the degree-1 displacement using the Australian GPS data. Such degree-1 displacement data (GPS minus GRACE) were further analyzed to determine the degree-1 geopotential coefficients or CM (7)–(9).

In this study, we rigorously combine GPS 3D deformation and GRACE geoid change data to determine all geopotential coefficients from degree 1, considering variance-covariance matrices of two different data sets. The result is a simultaneous solution of independent geocenter motion and gravity field change potentially improved by dense GPS network data. The final gravity field solutions are provided in the reference frame (ITRF) consistent with GPS data and more readily available for comparison with other geophysical models and data.

2.2. Linear Models of GPS and GRACE Data

Equations (2)–(4) for GPS observation can be written by separating the degree-1 terms from others as follows:

$$\mathbf{y} = \mathbf{A}_1\boldsymbol{\xi}_1 + \mathbf{A}_2\boldsymbol{\xi}_2 + \mathbf{e}, \tag{10a}$$

$$E\{\mathbf{e}\} = \mathbf{0}, D\{\mathbf{e}\} = \sigma^2\mathbf{P}^{-1}, \tag{10b}$$

where $\mathbf{y}$ includes 3D GPS displacement data at each station, $\boldsymbol{\xi}_1$ includes the geopotential coefficients for $l \geq 2$ and $\boldsymbol{\xi}_2$ has only the coefficients of $l = 1$, and $\mathbf{e}$ is a vector of GPS observation error. The expectation $E\{\mathbf{e}\}$ and dispersion $D\{\mathbf{e}\}$ of the GPS data error are described in equation (10b). The variance-covariance matrix (or weight matrix, $\mathbf{P}$) is typically available at every station with GPS data from the analysis centers. The matrices $\mathbf{A}_1$ and $\mathbf{A}_2$ are found from equations (2)–(4).

In this study, we use daily GPS position solutions and the variance-covariance matrices processed by Jet Propulsion Laboratory (JPL) (Heflin et al., 2018). They are available from nearly 3,000 continuously operating stations. The position solutions are referenced to International Terrestrial Reference Frame in 2008 (ITRF2008). Currently, the origin of ITRF2008 is defined to be the long-term mean CM realized by averaging Satellite Laser Ranging (SLR) solutions (Altamimi et al., 2016). This is different from the center of figure only by a constant offset (i.e., no temporal change) (Wu et al., 2012). After averaging daily solutions to monthly samples, the monthly mean displacement data sets and the corresponding variance-covariance matrices are used in equation (10), to be consistent with the GRACE data's temporal resolution.

The GRACE Level-1B (L1B) data (e.g., satellite tracking, accelerometer, and star camera data) were reduced to form the least-squares normal equations for global geopotential fields. The GRACE Level-2 (L2) solutions include monthly mean geopotential coefficients for $l \geq 2$ and their variance-covariance matrix. The L2 data products are available from April in 2002 to June 2017 with occasional data gaps. Such GRACE L2 data form a set of stochastic constraint equations as follows:

$$\mathbf{z} = \boldsymbol{\xi}_1 + \mathbf{e}_0, \tag{11a}$$

$$E\{\mathbf{e}_0\} = \mathbf{0}, D\{\mathbf{e}_0\} = \sigma^2\mathbf{P}_0^{-1}, \tag{11b}$$

where $\mathbf{z}$ includes GRACE measurements of the geopotential coefficients from degree 2, $\boldsymbol{\xi}_1$, with the associated error $\mathbf{e}_0$. The variance-covariance matrices of the monthly GRACE L2 solutions are also available from GRACE data processing centers.

We use the GRACE L2 data products processed by Institute of Theoretical Satellite Geodesy (ITSG) at Technical University of Graz. ITSG L2 data are in the form of the least-squares normal matrix $\mathbf{N}_g$ and the

associated vector $\mathbf{c}_g$ for monthly mean geopotential coefficients $\boldsymbol{\xi}_1$ (for $l \geq 2$) after backsubstituting the arc-dependent parameters (e.g., accelerometer biases and initial states) and daily gravity parameters (Mayer-Gürr et al., 2016). Their L2 data are computed up to degree and order 90 and the high-frequency atmosphere and ocean mass changes were removed using Atmosphere and Ocean Dealiasing (AOD) models (Dobslaw et al., 2013). Using these data sets, we found the GRACE measurement from $\mathbf{z} = \mathbf{N}_g{}^{-1}\mathbf{c}_g$ with its variance-covariance matrix $D\{\mathbf{e}_0\} = \sigma^2\mathbf{N}_g{}^{-1}$ (and $\mathbf{P}_0 = \mathbf{N}_g$) in equations (11a) and (11b).

2.3. A Combined Linear Model and the Least-Squares Solution

Next, we solve for the observation equation (10) under the a priori stochastic constraint equation (11) to find the combined solutions of the geopotential coefficients from GPS and GRACE data. We treat GRACE data (in the CM reference frame) as the "partial" stochastic information of the geopotential field defined in the reference frame consistent with GPS displacement data. It can be proven that the effect of the origin translation (within 1 cm) between the CM reference frame and ITRF on the higher-degree geopotential coefficients is negligible, for example, 8–9 orders of magnitude smaller for degree-2 coefficients. This means that the GRACE data in the CM reference frame can be considered as the higher-degree ($l \geq 2$) geopotential data in ITRF. This problem of solving observation equations with partial stochastic constraints is often referred to as least-squares collocation according to Wolf (1977), or equivalently, an extended Gauss-Markov model with a priori information by Koch (1999).

Combining the observation equation (10) and the partial stochastic information equation (11), we have

$$\begin{bmatrix}\mathbf{y}\\ \mathbf{z}\end{bmatrix} = \begin{bmatrix}\mathbf{A}_1 & \mathbf{A}_2\\ \mathbf{I} & \mathbf{0}\end{bmatrix}\begin{bmatrix}\boldsymbol{\xi}_1\\ \boldsymbol{\xi}_2\end{bmatrix} + \begin{bmatrix}\mathbf{e}\\ \mathbf{e}_0\end{bmatrix}, \tag{12a}$$

$$E\left\{\begin{bmatrix}\mathbf{e}\\ \mathbf{e}_0\end{bmatrix}\right\} = \mathbf{0}, D\left\{\begin{bmatrix}\mathbf{e}\\ \mathbf{e}_0\end{bmatrix}\right\} = \sigma^2\begin{bmatrix}\mathbf{P}^{-1} & \mathbf{0}\\ \mathbf{0} & \mathbf{P}_0^{-1}\end{bmatrix}. \tag{12b}$$

A combined normal equation is obtained as

$$\begin{bmatrix}\mathbf{A}_1^T\mathbf{P}\mathbf{A}_1 + \mathbf{P}_0 & \mathbf{A}_1^T\mathbf{P}\mathbf{A}_2\\ \mathbf{A}_2^T\mathbf{P}\mathbf{A}_1 & \mathbf{A}_2^T\mathbf{P}\mathbf{A}_2\end{bmatrix}\begin{bmatrix}\widehat{\boldsymbol{\xi}}_1\\ \widehat{\boldsymbol{\xi}}_2\end{bmatrix} = \begin{bmatrix}\mathbf{A}_1^T\mathbf{P}\mathbf{y}+\mathbf{P}_0\mathbf{z}\\ \mathbf{A}_2^T\mathbf{P}\mathbf{y}\end{bmatrix}. \tag{13}$$

The variance component of the combined solution is computed as

$$\widehat{\sigma}^2 = \frac{\widetilde{\mathbf{e}}^T\mathbf{P}\widetilde{\mathbf{e}} + \widetilde{\mathbf{e}}_0^T\mathbf{P}_0\widetilde{\mathbf{e}}_0}{n-m+r} = \frac{\mathbf{y}^T\mathbf{P}\left(\mathbf{y}-\mathbf{A}_1\widehat{\boldsymbol{\xi}}_1-\mathbf{A}_2\widehat{\boldsymbol{\xi}}_2\right) + \mathbf{z}^T\mathbf{P}_0\left(\mathbf{z}-\widehat{\boldsymbol{\xi}}_1\right)}{n-m+r}, \tag{14}$$

where n is the number of observations, m is the number of unknowns, and r is the number of constraints. By putting $\mathbf{z} = \mathbf{N}_g{}^{-1}\mathbf{c}_g$ and $\mathbf{P}_0 = \mathbf{N}_g$ from the GRACE L2 data products, we obtain the least-squares solutions of

$$\begin{bmatrix}\widehat{\boldsymbol{\xi}}_1\\ \widehat{\boldsymbol{\xi}}_2\end{bmatrix} = \begin{bmatrix}\mathbf{A}_1^T\mathbf{P}\mathbf{A}_1 + \mathbf{N}_g & \mathbf{A}_1^T\mathbf{P}\mathbf{A}_2\\ \mathbf{A}_2^T\mathbf{P}\mathbf{A}_1 & \mathbf{A}_2^T\mathbf{P}\mathbf{A}_2\end{bmatrix}^{-1}\begin{bmatrix}\mathbf{A}_1^T\mathbf{P}\mathbf{y}+\mathbf{c}_g\\ \mathbf{A}_2^T\mathbf{P}\mathbf{y}\end{bmatrix}, \tag{15}$$

and, its variance-covariance matrix of

$$D\left\{\begin{bmatrix}\widehat{\boldsymbol{\xi}}_1\\ \widehat{\boldsymbol{\xi}}_2\end{bmatrix}\right\} = \widehat{\sigma}^2\begin{bmatrix}\mathbf{A}_1^T\mathbf{P}\mathbf{A}_1 + \mathbf{N}_g & \mathbf{A}_1^T\mathbf{P}\mathbf{A}_2\\ \mathbf{A}_2^T\mathbf{P}\mathbf{A}_1 & \mathbf{A}_2^T\mathbf{P}\mathbf{A}_2\end{bmatrix}^{-1}, \tag{16}$$

where

$$\widehat{\sigma}^2 = \frac{(\mathbf{P}\mathbf{y})^T\left(\mathbf{y}-\mathbf{A}_1\widehat{\boldsymbol{\xi}}_1-\mathbf{A}_2\widehat{\boldsymbol{\xi}}_2\right) + \mathbf{c}_g{}^T\left(\mathbf{z}-\widehat{\boldsymbol{\xi}}_1\right)}{n-m+r}. \tag{17}$$

Finally, we have $\widehat{\boldsymbol{\xi}}_2$ for the geocenter motion solution (geopotential coefficients for $l = 1$) and $\widehat{\boldsymbol{\xi}}_1$ for the geopotential fields (for $l \geq 2$) improved by GPS data from the original GRACE solution $\mathbf{z}$. Next, we assess these

solutions with other independent estimates and discuss the effect of GPS data to GRACE solutions and the importance of uncertainty in geocenter motion for water storage computation.

3. Results

3.1. GPS Site Selection and Pre-processing

Daily solutions of 3D GPS positions and their covariance matrices from the Jet Propulsion Laboratory (JPL) *rp2011b* product release were used in the analysis (Heflin et al., 2018). Solutions spanning the time period from 2003 to 2016, which included 2,703 unique sites, were selected to overlap with the GRACE mission L2 geopotential field products. The 3D position vectors in this solution are referenced to ITRF2008 (Heflin et al., 2018). Displacements caused by solid Earth, pole tide, and ocean tide loading were removed following International Earth Rotation and Reference System Service (IERS) Conventions 2010 (Petit & Luzum, 2010), consistent with GRACE data processing for modeling the tidal effects. Prior to combination with the GPS deformation fields, the GRACE L2 geopotential field solutions were corrected for signals not related to elastic loading deformation including tidal deformation, GIA, earthquakes, and tectonic effects (Chao, 2016).

The JPL GPS solutions are provided with the estimates of "breaks" or offsets in the GPS time series, often caused by instrumental changes as well as geophysical events like earthquakes. The amplitude of these position offsets were statistically estimated along with timings of the breaks and provided as corrections to rp2011b position solutions (Heflin et al., 2018). We applied these corrections to remove these identified offsets in the GPS time series. These corrections effectively eliminate the coseismic deformation from the GPS data. We modeled monthly elastic and viscoelastic geoid changes after the 10 largest great earthquakes during the period (an update from Han et al. (2013) and Han et al. (2019)) to remove undesired earthquake effects from GRACE data. We also removed the viscoelastic deformation signals from the vertical GPS data based on a GIA model by Caron et al. (2018) and the corresponding geoid change from GRACE data.

Furthermore, we eliminated linear trends from the east and north GPS time series components to compensate for tectonic plate motion. Any horizontal elastic deformation associated with secular change in surface mass loading, generally two orders of magnitude smaller than the plate motion, is also removed by this detrending, which will essentially limit the application of GPS horizontal data to determine secular change in geocenter motion. Finally, we computed weighted monthly mean displacements and their variance-covariance matrices from daily time series of displacements and variance-covariance matrices. The mean GPS position vectors and the GRACE gravity field averaged over the period of 2003 to 2016 were then removed from each of the GPS and GRACE time series. Each data set refers to the monthly anomaly with respect to the study period of 2003 to 2016.

Once the above pre-processing is complete, we pre-screened GPS sites to retain only the sites reflecting the elastic response to surface mass. First, we computed the elastic deformation from GRACE geoid changes and SLR geocenter motion solutions at all GPS sites and, then, we omitted the sites presenting a negative correlation between GPS measurements and the GRACE + SLR computed deformation. This pre-screening based on a simple correlation analysis effectively identifies the stations of which vertical deformation is positively correlated with geoid changes (i.e., deformation not associated with elastic loading). This analysis identified sites in the Central Valley, California with a dominantly poroelastic response and Long Valley caldera and Yellowstone associated with volcanic activity. A thorough and comprehensive examination of the western U.S. GPS sites regarding non-elastic loading signals was conducted by Argus et al. (2017) based on local geologic information.

Now, we assume that the remaining GPS displacements are predominantly caused by surface mass loading due to hydrology, atmosphere, and non-tidal ocean mass changes and that the major effect of the non-surficial processes such as GIA, earthquakes, and tectonics are eliminated from both the GPS and GRACE solutions. To be consistent with GRACE data in terms of geophysical signal content, we additionally removed the elastic deformation predicted from atmosphere and ocean mass loading based on the AOD data products from the monthly mean GPS data.

Finally, we selected only GPS sites with time series longer than five years (between 2003 and 2016) and with less than 50% data gaps. Sites showing excessive secular vertical motion (>4 mm/year) were also excluded as these sites when investigated have often been found be undergoing deformation related to local sources

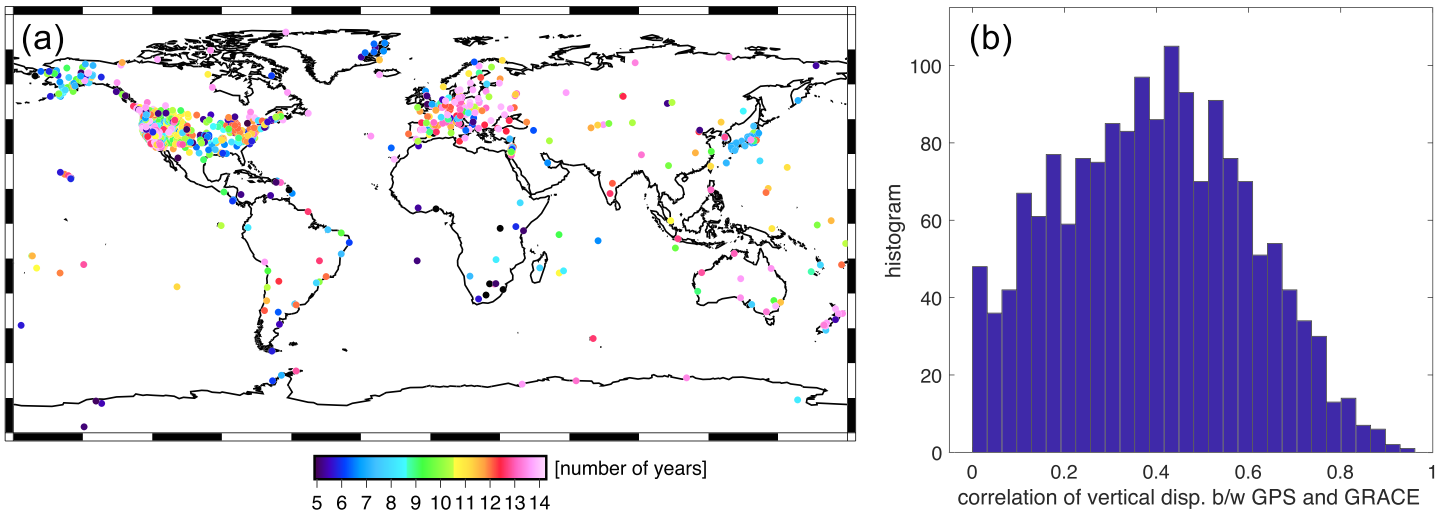

Figure 1. (a) Spatial locations of GPS sites used in this study; of the 2,703 sites available, 1,651 stations satisfied our criteria for use in the study. The color indicates the number of years in the time series available from 2003 to 2016. (b) Histogram of the cross correlation of vertical deformation time series between GPS and GRACE.

inconsistent with regional deformation or are the result of defective equipment. After pre-screening and applying these selection criteria, we were left with a total of 1,651 sites out of a total of 2,703 originally considered (a list of selected GPS site names and coordinates is provided in the supporting information). Figures 1a and 1b, respectively, present the geographical locations of GPS stations used in this study with the total number of available data at each station depicted by different colors and the histogram of cross correlation of vertical deformation time series between GPS and GRACE. For example, nearly 1,100 stations exhibit correlation greater than 0.3 in the vertical time series.

3.2. GPS and GRACE Joint Inversion

The monthly averaged GPS displacement data were expanded in terms of a spherical harmonic series from degree and order 1 to 90. The maximum degree 90 is commensurate with ITSG's GRACE normal equation data sets. Analysis of global land surface models indicate the omission error (contribution beyond degree 90) is relatively small (less than 1% of total signal) excluding the cases of elastic response to locally intense loads such as dams and lakes (Han, 2016). GPS normal equation matrices and vectors were accumulated from the monthly averaged GPS time series selected according to the criteria discussed above. The full covariance information for the 3D displacements at each site and every epoch were incorporated, but no intra-station covariance between stations was considered. Since estimates of geocenter motion have previously been found to be more sensitive to horizontal than vertical displacements (see Figure 9 of Han (2016) and Figure 2 of Chanard et al. (2018)), we computed two sets of GPS normal equations, one set using only the horizontal GPS displacements and the other set using the full 3D displacement vectors, and compared the results.

To illustrate the relative contribution of the degree-1 and higher degrees, we computed the elastic load displacement using the geopotential coefficients from SLR degree-1 and from GRACE for degrees from 2 to 40, separately. The left panels of Figure 2 present the root-mean-square (RMS) variability of displacement from degree-1 only (SLR) relative to that from degrees 2–40 (GRACE). The right panels show an example displacement time series computed from SLR and GRACE at ALIC (Alice Springs, central Australia). We observe that, in many locations globally, the degree-1 displacements are found to be as large as 70% of all other degrees combined ($l \geq 2$) in east displacement and even larger (>100%) in north displacement. For the vertical component however, the degree-1 contribution is mostly 20% or less at most locations except Europe, New Zealand where the degree-1 displacement can be up to ~50% of other degrees (we will discuss this in detail later). This is the reason why the geocenter motion can be derived from horizontal displacement alone.

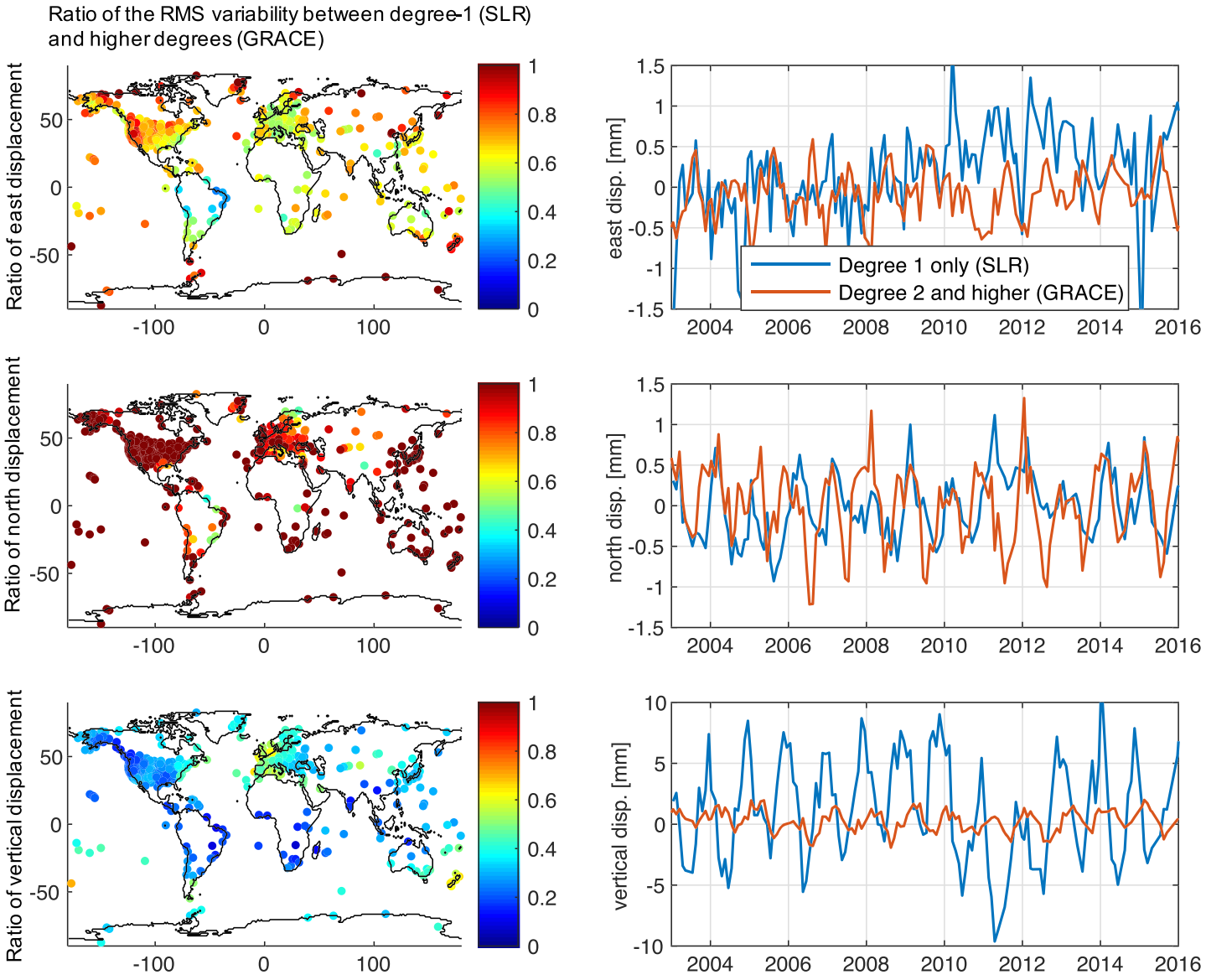

Figure 2. Left columns present the ratio of RMS variability of the degree-1 ($l = 1$) displacement to that of other degrees ($l \geq 2$) in east, north, and vertical displacement, respectively, in top, middle, and bottom panels. The degree-1 displacement was computed from SLR solutions and other degrees were from GRACE solutions of geopotential change. Right columns show an example time series from SLR degree-1 and GRACE geopotential data evaluated at a GPS site, ALIC (Alice Spring, Australia). There is an order of magnitude difference in computed displacement between horizontal and vertical components.

We constructed the combined normal equations by adding monthly GRACE data ($\mathbf{N}_g$ and $\mathbf{c}_g$) to GPS normal equations and inverted the combined normal matrix as shown in equation (15). The geopotential field solutions for a total of 150 months were estimated every month from January 2003 to December 2016 (excluding the months where no GRACE data were available). The variance-covariance matrix of the solution was also computed following equation (16) by propagating the original variance-covariance matrices of GRACE and GPS data. The variance components were estimated from equation (17) and they exhibited estimates within the range of 1–3 for the entire period, confirming that the a priori weightings applied to GPS and GRACE data were reasonable.

3.3. Solutions of Geocenter Motion (Degree-1 Geopotential Coefficients)

We compared our monthly degree-1 geopotential solutions determined from the joint inversion of GPS and GRACE data with solutions obtained from (1) the analysis of tracking five SLR satellites (LAGEOS-1

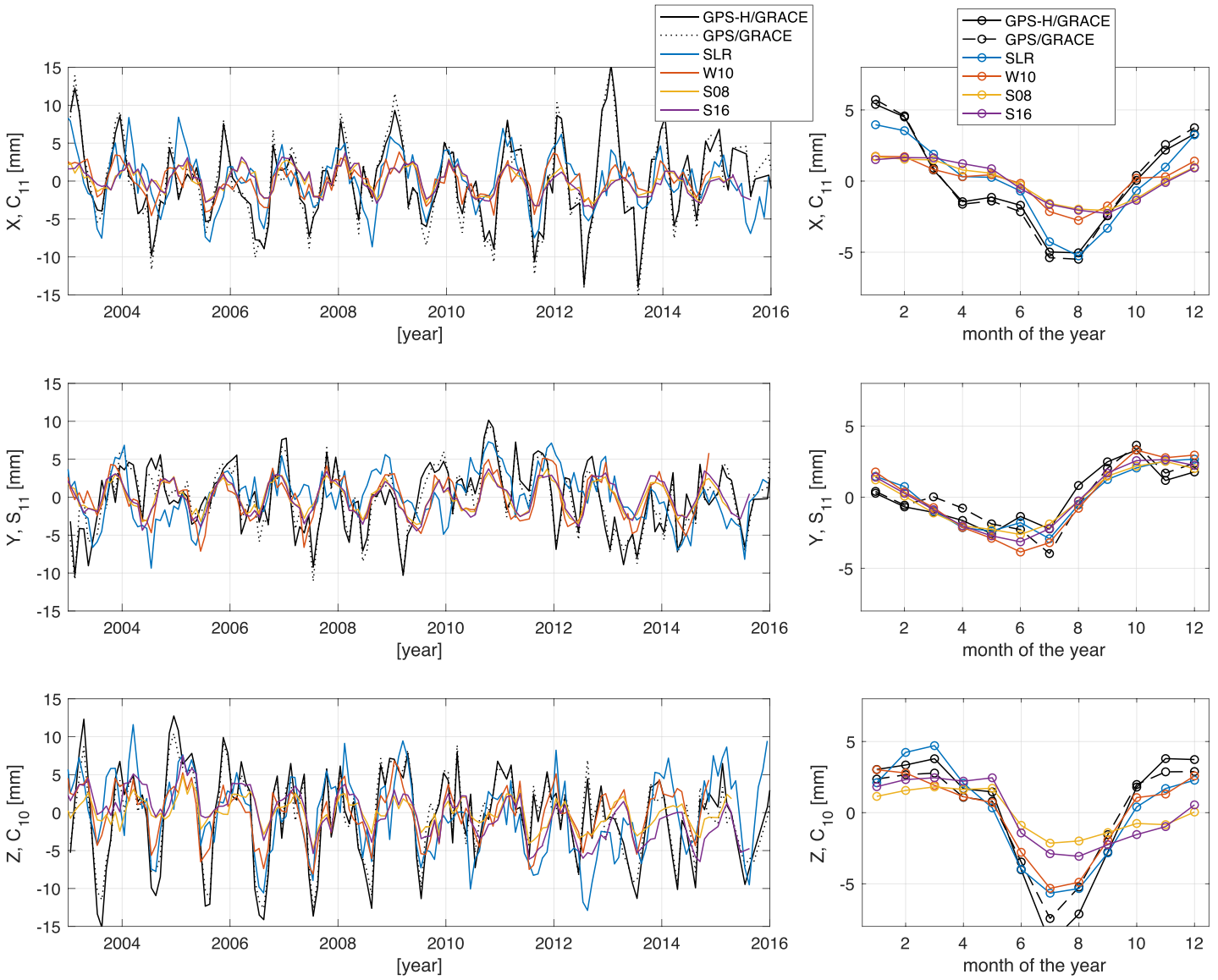

Figure 3. Geocenter motion (i.e., degree-1 geopotential) solutions from five different methods including (1) a joint inversion of horizontal GPS data and GRACE (GPS-H/GRACE) and (2) of 3D GPS and GRACE data (GPS/GRACE), both from this study; (3) SLR data analysis; (4) global inverse approach (W10); and (5) GRACE and ocean model analysis (S08) and its update considering SAL (S16). The monthly time series of X, Y, and Z components from each method are shown for 2003 to 2016 in left columns. The average monthly variations stacked over 2003–2016 are presented in right columns. All solutions are most consistent in Y component, while GPS/GRACE solutions compare best with SLR observations in other components. GPS horizontal displacement is more critical to constrain geocenter motion when combined with GRACE.

and 2, Starlette, Stella, and Ajisai) (Cheng et al., 2013), (2) the global inverse approach using GRACE, GPS, and ocean bottom pressure data sets, W10 (Wu et al., 2010), and (3) the analysis of ocean models and GRACE data, S08 (Swenson et al., 2008). Figure 3 compares these time series of degree-1 geopotential including our GPS/GRACE solutions from horizontal GPS displacement data only and from 3D GPS displacements, in terms of the CM coordinates following equation (6). Clearly, the geocenter motion is already well recovered when only the horizontal GPS data are used (1.1–1.5-mm RMS difference with the solutions obtained using the 3D GPS data). This result substantiates the finding of others (Chanard et al., 2018; Han, 2016) that the contribution of the vertical GPS displacement data to the degree-1 solutions is secondary.

The X component of geocenter motion shows an overall seasonal variation within ±5 mm (see the right panels of Figure 3 showing a 13-year average monthly change). The GPS/GRACE solutions more closely follow the SLR solutions than the other solutions in X component. The W10 and S08 solutions are in phase with GPS/GRACE and SLR solutions but the amplitude of the X coordinates is 50% smaller. The GPS/GRACE solutions show unusually large variations in X components relative to other solutions during 2011–2013. According to a sensitivity analysis by Han (2016), the X component of geocenter motion is most effectively constrained by *east* displacement from U.S. stations (see Figure 9 of Han, 2016). Indeed, we found the majority of the western and Central U.S. sites present larger seasonal change in east displacement during 2011–2013 (see Figure 6 for an example of STLE).

The Y component of geocenter motion shows an overall seasonal variation within ±3 mm. All solutions are most consistent in this component (yielding >90% correlation and <1 mm difference in seasonal change). The Y component of geocenter motion is effectively constrained by *north* displacement of the U.S. stations (see also Figure 6 showing that the north GPS displacement basically agrees with the geocenter motion).

The largest variability of geocenter motion is found in the Z component showing an overall seasonal change within a range of −7 to +4 mm. Note that the seasonal anomaly is quite different from a simple sinusoid, showing the intense negative change over four months (June to September) and a moderate positive change for eight months. The Z components are constrained by north displacement of GPS sites in low- and middle-latitude regions and the by the vertical displacement in polar regions. It is also noted that east GPS displacement are not sensitive to the Z component of geocenter motion (Figure 9 of Han (2016)). Considering the spatial distribution of GPS stations used in this study, the Z components would have been constrained mostly by north displacement in United States, Europe, and Japan. All GPS/GRACE, SLR, and W10 solutions agree in amplitude, phase, and pattern of the seasonal change. However, the S08 solutions are smaller by a factor of 2–3 and their seasonal patterns are quite different from other solutions, leading to the negative anomalies spread over an extended period from June to December. Unlike other solutions based on geodetic observations, the S08 solutions rely on the ocean model outputs that disregarded the effect of ocean's self-attraction and loading (SAL) (Clarke et al., 2005). The recent update to S08 by Sun et al. (2016) including SAL (or passive ocean response), shown as S16, is not different from S08 except a slight increase in Z component amplitude.

The power spectral density (PSD) of the geocenter motion time series is presented in Figure 4. The periods corresponding to the annual cycle and its overtones and the GPS draconitic period (~351 days) (Griffiths & Ray, 2013) and its overtones are illustrated with vertical colored lines. The GPS/GRACE solutions show spurious power at periods of 250–340 days in the X component. In addition, the GPS/GRACE solutions also contain power at multiple overtones of the GPS draconitic period while the other non-GPS solutions in comparison do not. These spurious systematic draconitic signals are inherent at various levels in all GPS time-series; they originate as a result of mis-modeling of solar radiation pressure effects on GPS orbits and are not indicative of geophysical signals (Griffiths & Ray, 2013; Ray et al., 2008; Rodriguez-Solano et al., 2014). These draconitic errors may be regionally-correlated if they originated from the orbit error and contaminate the degree-1 geopotential estimation. Around the annual period, GPS/GRACE and SLR solutions agree in amplitude while W10 and S08 are 2 times smaller in the X component. All four solutions agree in the Y component. Whereas, the S08 solution shows only about half of the amplitude of the other three solutions in the Z component. Unlike other solutions, GPS/GRACE solutions exhibit spurious power at the draconitic period and its overtones account for less than 20% of the total signal in amplitude.

In order to assess the impact of our degree-1 solutions on the GPS measurements, we computed monthly displacement time series using (1) GRACE geopotential coefficients ($l \geq 2$) only, (2) GRACE + SLR degree-1 coefficients, and (3) GRACE + our GPS/GRACE degree-1 solutions, and compared with the monthly time series of GPS observations. Figure 5 shows the cross correlation between the calculated displacements and GPS data at all of the subsetted 1,651 stations. The histogram of the correlations is shown in top panels, for the east, north, and vertical displacements. The median values of correlation between GPS and GRACE time series (i.e., no degree-1 coefficients) are 0.10, 0.27, and 0.44, for east, north, and vertical displacement, respectively. Cross correlations increased to 0.20, 0.43, and 0.44 between GPS and GRACE + SLR degree-1, while replacing the degree-1 components with our GPS/GRACE solutions, they become 0.62, 0.69, and 0.47. The correlations between GPS data and the computed displacement were significantly

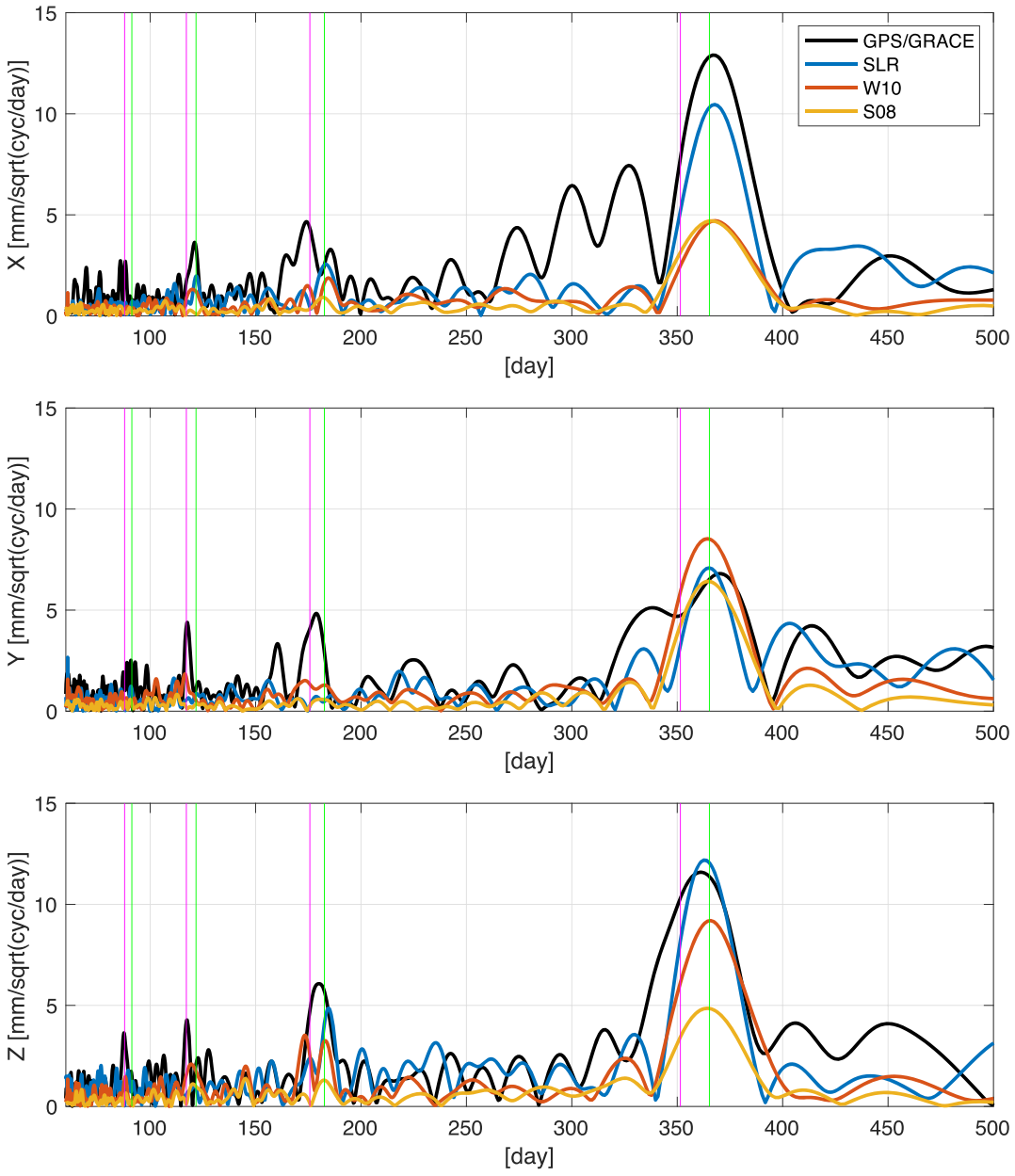

Figure 4. Different solutions of geocenter motion were compared in terms of amplitude spectral density (mm/$\sqrt{\text{cycle/day}}$). The green vertical lines indicate the annual period (365.25 days) and its overtones while magenta lines indicate the GPS draconitic period (351 days) and its overtone. Unlike other solutions, GPS/GRACE solutions exhibit spurious power at the draconitic period and its overtones.

improved by adding the degree-1 displacement to the GRACE-inferred displacement, in other words, by making the reference frame consistent between GRACE and GPS data, for east and north displacements. However, there is little impact of the degree-1 coefficients on vertical displacement. This confirms the findings of Han (2016) and Chanard et al. (2018) that the effect of the degree-1 surface mass load is larger on horizontal displacement than vertical displacement.

The horizontal displacements computed using our GPS/GRACE solutions of degree-1 agree significantly better with the observed GPS time series than the time series derived using SLR degree-1 (0.20 versus 0.62 for east and 0.43 versus 0.69 for north). The improvement is found most evident in the United States where

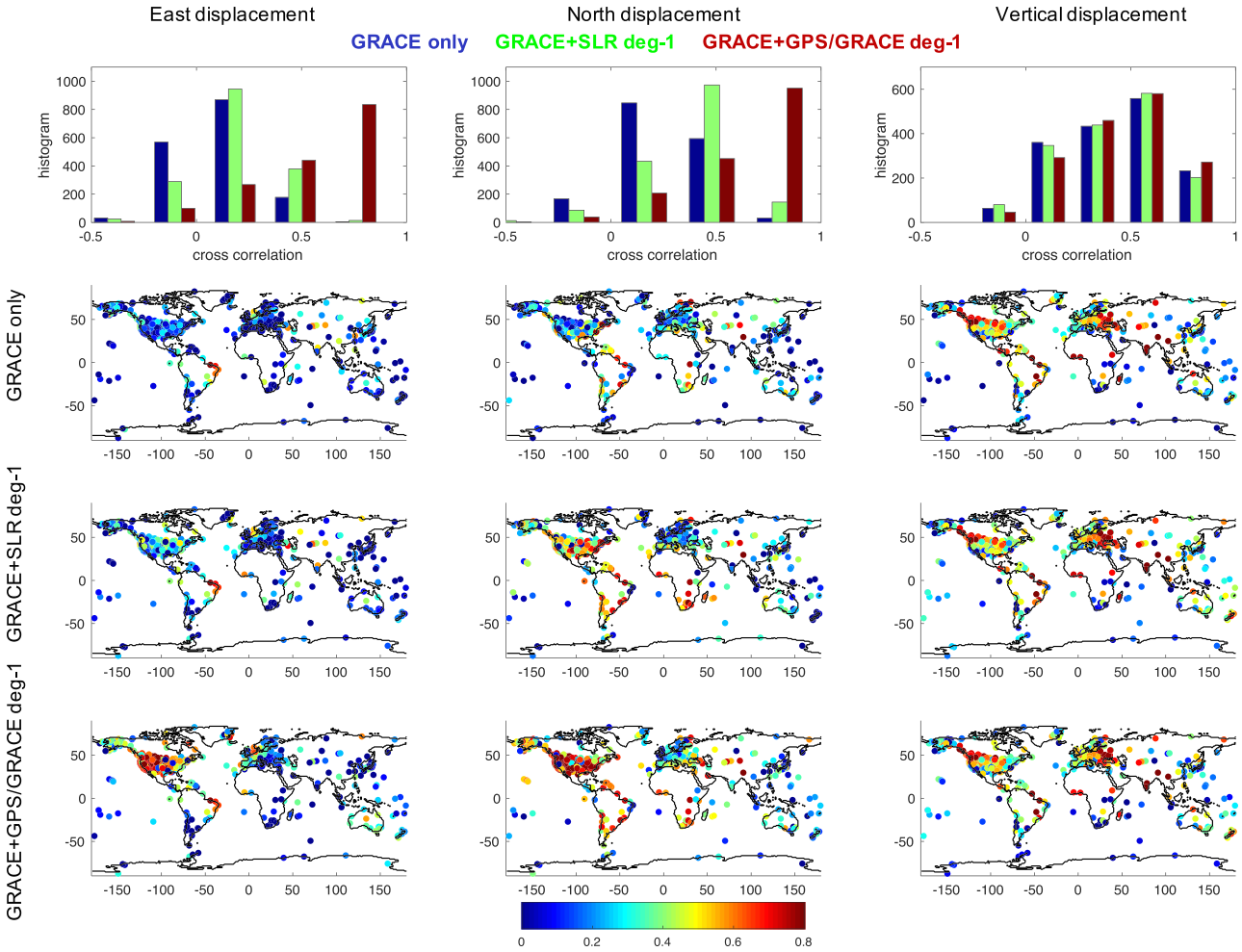

Figure 5. Cross correlation between GPS measured displacement and the computed displacement from GRACE geopotential data ($l \geq 2$) only, GRACE + SLR degree-1 coefficients, and GRACE + degree-1 solution from this study. The effect of degree-1 coefficients is larger in the horizontal displacement.

there are correlations of 0.6 and greater for most stations and also in Europe. However, this does not mean that our GPS/GRACE geocenter motion solutions are better than the SLR solutions. The better correlations are rather expected since the GPS data were used in our solutions of geocenter motion. Any spatially-correlated error in the GPS data (such as the spurious signals at the draconitic period) is propagated into our degree-1 solutions leading to our solutions comparing better with GPS data.

An example GPS time series from STLE in the Central United States is shown in Figure 6. The GPS data were compared with the predicted displacements using the degree-1 coefficients from SLR and our GPS/GRACE solutions and using other higher degrees (greater than and equal to 2) from GRACE + AOD model. The measured horizontal GPS displacements are correlated with the computed displacements from the degree-1 (geocenter motion) coefficients, while the vertical displacements are correlated with the synthetic data computed from higher-degree GRACE + AOD coefficients. It demonstrates that the seasonal horizontal displacement of the Earth's surface are largely driven by seasonal migration of the centroid (degree-1) of global surface mass including atmospheric, oceanic, and hydrological masses.

The spatial patterns of the degree-1 displacements were computed at each of GPS stations. Figure 7 illustrates the seasonal 3D deformation caused by the degree-1 load from SLR (top) and our GPS/GRACE solutions (bottom). During December–January, both solutions found that the North American continent moves northeast and subsides, Australia and New Zealand shift northwest and uplift, and Africa moves northward by a couple of mm. The European sites subside collectively; however, their horizontal motion looks complicated. Our GPS/GRACE solution predicts larger deformation than the SLR solution does, as expected from

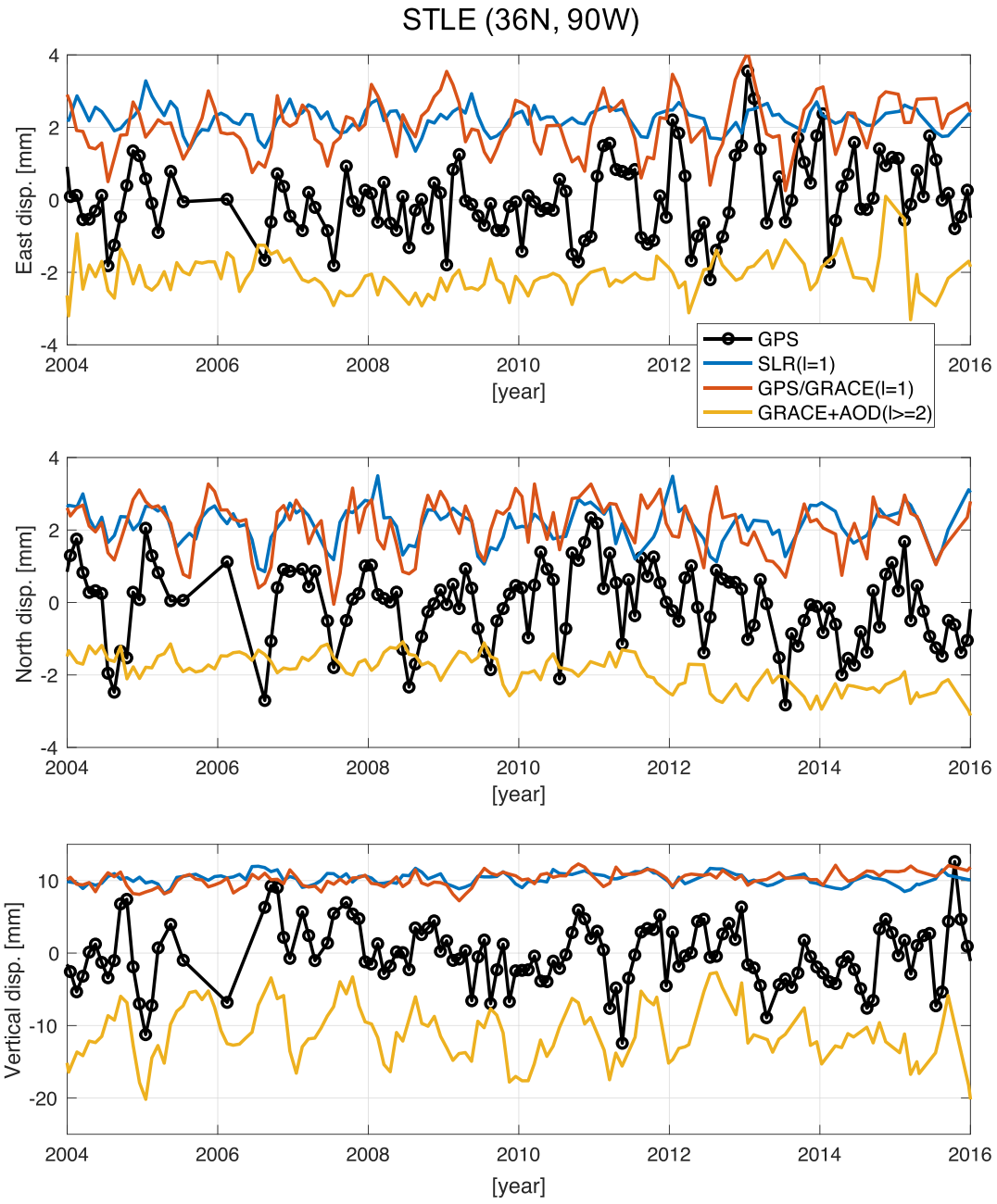

Figure 6. Monthly time series of GPS (north, east, up) displacements for site STLE (black), degree-1 (X, Y, Z) displacements computed from SLR (blue) and from this study (red), and displacement computed from GRACE + AOD model for higher degrees of $l \geq 2$ (yellow). The GPS site STLE located in the Central United States. The horizontal GPS displacement data are correlated in terms of amplitude and phase with the degree-1 displacement while the vertical GPS data are correlated with the higher-degree components from GRACE. This figure demonstrates how GPS horizontal displacements in U.S. sites closely follow the displacement associated with geocenter motion (degree-1 load migration).

Figure 3. During June–July (six months later), the opposite patterns of 3D deformation were observed from both SLR and GPS/GRACE degree-1 solutions.

The degree-1 horizontal displacement is larger in the United States than in Europe, while its vertical deformation is larger in Europe than in the United States. Because the degree-1 horizontal signals are larger in the

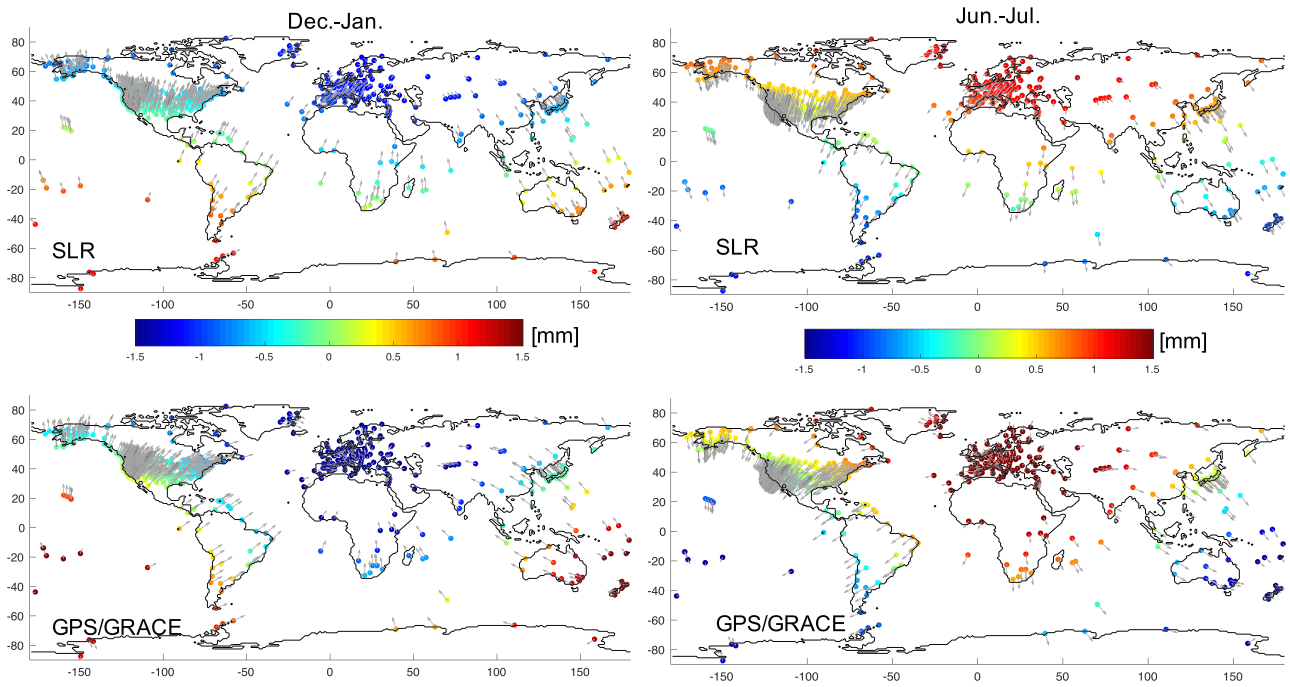

Figure 7. (top panel) The degree-1 displacement inferred from SLR solutions and (bottom panel) the GPS/GRACE displacement estimated in this study. The seasonal deformation predicted in the beginning of the year and in the middle of year are presented. For example, the conterminous United States moves northeast during December–January, while it moves southwest during June–July. Such motion identifies the centroid of positive surface mass redistribution in Europe during December–January and in the South Pacific during June–July (see Figure 12).

United States, the correlation between GPS measurements and the computed degree-1 horizontal displacements is higher in the United States than in Europe (as seen in Figure 5). The subsidence of Europe in the beginning of year and the subsidence of New Zealand in the middle of year imply the overall trajectory of the degree-1 surface mass migration from Europe to South Pacific.

3.4. Solutions of Geopotential Field (Higher Degrees)

We evaluated the other set of geopotential coefficients at degrees higher than or equal to 2 from our joint GPS/GRACE inversion (with 3D GPS data) and compared them with the GRACE only solutions to quantify the effect of GPS data at higher degrees and orders. Unlike the geocenter motion solutions, the vertical GPS data are important to constrain higher-degree components. The degree variances were computed every month for total 150 months and averaged over the entire period from 2003 to 2016. Figure 8 depicts the average of degree RMS (square root of degree variance) of the geopotential coefficients as a function of degree (2–90). In general, when GPS data were incorporated, the variances of the geopotential solutions were reduced for degrees greater than 30 where the noise exceeds the signals in a global average sense.

The effects of GPS data were examined for individual coefficients as well. First, we analyzed the monthly time series of the coefficients using a deterministic model composed of parameters for annual and semi-annual sinusoids, linear and quadratic trends, and a mean offset. Then, we computed variance reduction (R^2, R-squared) of each time series from GRACE-only and GPS + GRACE joint inversion solutions. The higher variance reduction implies that time series is more systematic (and less noisy) likely indicating improved solutions. For each geopotential coefficient, the R^2 of GRACE-only solution was subtracted from the R^2 of GPS + GRACE solution and the result was normalized (divided) by the R^2 of the GRACE-only solution. A quotient (Q) greater than 0 indicates that the time series became more systematic by virtue of GPS data, while the negative Q means that the time series became more random (noisier). A Q close to 0 indicates no change.

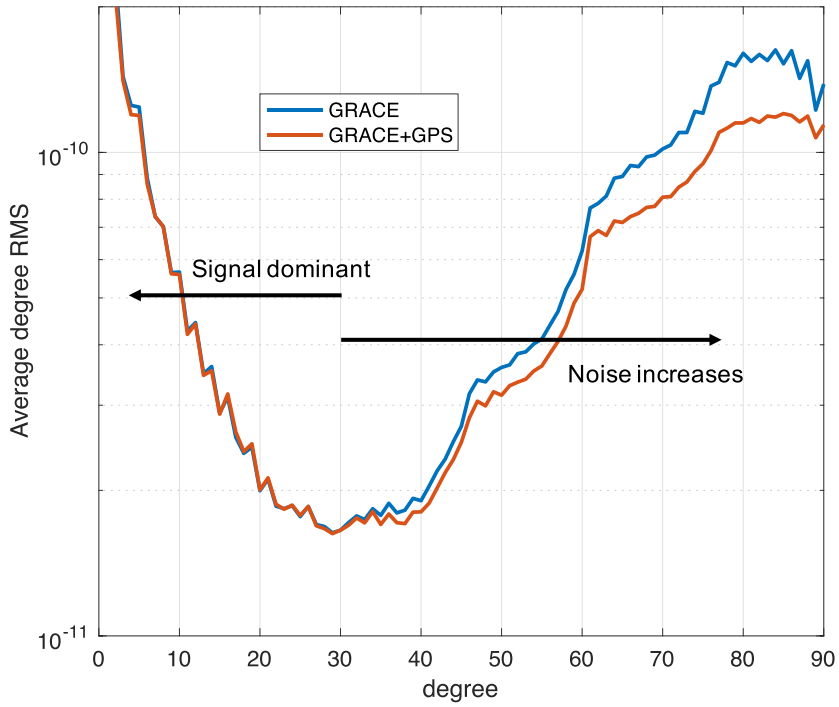

Figure 8. The average degree RMS of monthly geopotential solutions from a joint inversion of GPS and GRACE data from 2003 to 2016. Our new solutions were compared with the original GRACE only solutions. The new combination solution presents less RMS noise in the degree band higher than 30.

The top panel of Figure 9 shows Q for each geopotential coefficient (the average of 150 monthly solutions). It is seen that the coefficients at lower order ($m \leq$ ~16) were less affected by GPS data evidenced from Q ≈0 (green color in the figure), while the coefficients of higher order and degree became more systematic (red color) with inclusion of GPS data; there are some coefficients showing negative Q (blue color). However, most of the coefficients became more systematic after including GPS data. Such pattern of changes at different degree and order is explained readily by the uncertainty of GRACE solutions shown in bottom panel of Figure 9. The GRACE coefficients with larger uncertainty (higher-order coefficients) were changed more effectively by GPS data.

Figure 10 shows the time series of selected zonal coefficients from GRACE-only and GPS + GRACE solutions. It demonstrates that GPS data help to correct the noisy GRACE-only solutions at the lowest degree ($l = 2$) and higher degrees ($l \geq 19$), particularly during the months when GRACE satellites were in deep resonance yielding undesired repeat orbits.

The GRACE geopotential data have been used widely to quantify the basin-average water storage changes. We compared the results from GRACE-only and GPS + GRACE solutions for the Mississippi and Colorado River basins in the United States and the Danube river basin in Europe, where dense networks of GPS stations are available. No post-processing was applied to the geopotential solutions and a simple basin average was made in the computation. Figure 11 presents monthly time series of water storage changes at different basins computed from different spectral (degree) bands. The basin-averaged water storage variations computed from two solutions agree in the degree band of $2 \leq l \leq 60$, while over the smallest Colorado basin, the GRACE-only solutions are nosier than the GPS/GRACE solutions due to larger GRACE data noise in higher degrees that were not sufficiently averaged out over the Colorado basin (left panels of Figure 11). The GPS data cleaned up such noise in the high-degree GRACE solutions. This can be better seen by evaluating the storage changes at the degree band of $30 \leq l \leq 60$ (middle panels of Figure 11). Considerable noise was found in the GRACE-only solutions from all basins, while the GPS/GRACE solutions present seasonal and inter-annual changes with amplitudes of a few centimeters, highlighted by the black curves representing the least squares fit of seasonal and inter-annual trends.

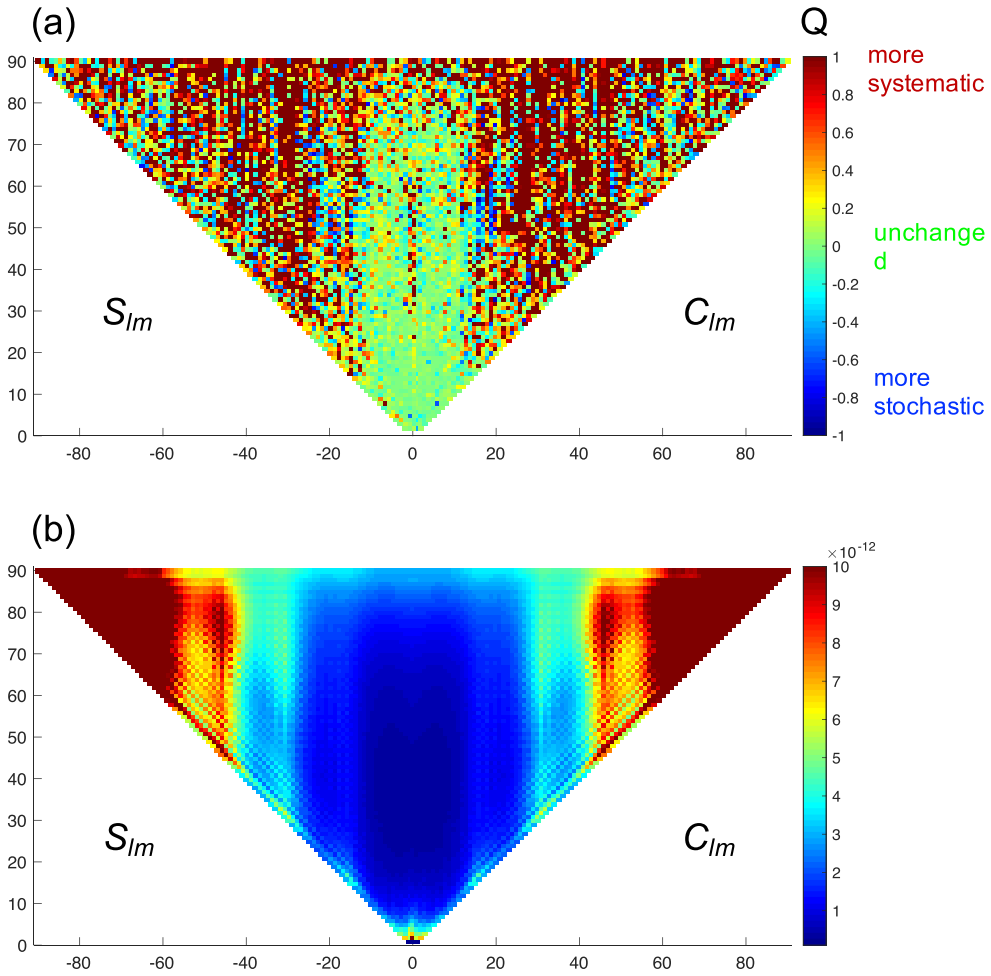

Figure 9. (a) The variance reduction quotient Q (see the exact definition in the text). The case of Q > 0 indicates the monthly time series of each coefficient become more systematic by virtue of inclusion of GPS data compared to the original GRACE time series. In contrast, Q < 0 implies the coefficients become more random due to the inclusion of GPS data. For most coefficients of higher order ($m > 16$), the time series of geopotential coefficients become more systematic (less noisy) with GPS data. (b) The standard error estimate of GRACE geopotential coefficients. The improvement by including GPS data is more evident where the uncertainty is larger.

We also evaluated two solutions at the degree band of $60 \leq l \leq 90$, where the GRACE data are too noisy (right panels of Figure 11). The GRACE-only solutions at those degrees cannot be used since the noise greatly exceed the signals; however, the GPS + GRACE solutions still exhibit systematic seasonal variation and inter-annual changes consistent with the results at the lower degree band ($30 \leq l \leq 60$). Although a rigorous validation is required to assess the potential signals found in the GPS + GRACE solutions beyond degree 60, our results in Figure 11 sufficiently demonstrate that the GPS data indeed reduced the GRACE data noise and increased the spatial resolution of the surface mass estimates.

3.5. Effect of Geocenter Motion on GRACE Surface Mass Estimates

We computed the spatial patterns of seasonal surface mass changes using the geopotential solutions. Figure 12 presents the cosine (in-phase) and sine (quadratic) components of seasonal changes: top row from our GPS/GRACE degree-1 coefficients, middle row from SLR degree-1, and bottom row from GRACE ($l \geq 2$). The seasonal change of the degree-1 mass load is as large as 3 cm in terms of equivalent water height. In the beginning of year, the positive anomaly appeared over Europe and the negative anomaly developed in the South Pacific Ocean (seen from the cosine component of seasonal change). Three months later, the positive anomaly shifted westward and developed over the North Atlantic Ocean with reduced intensity and,

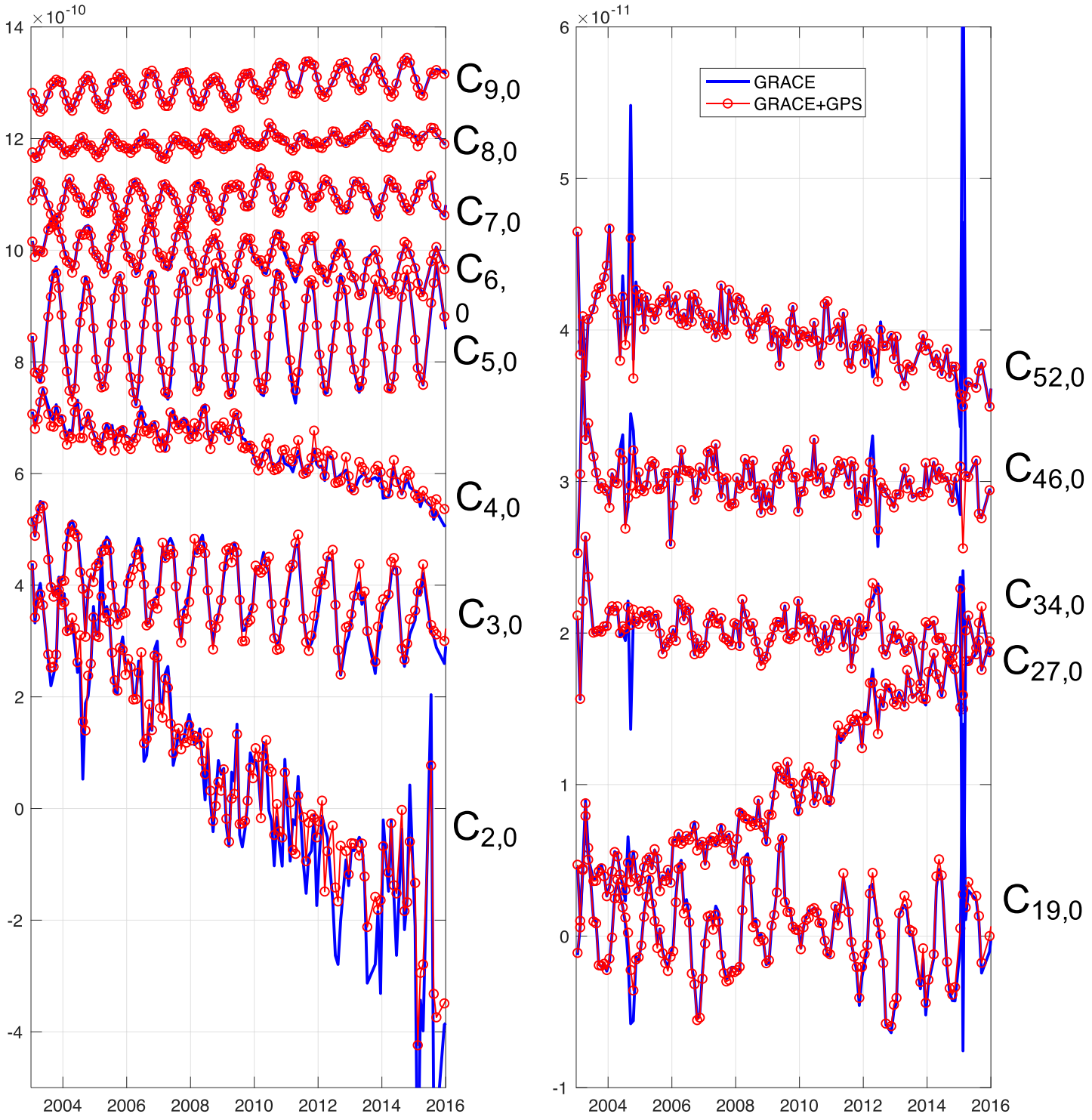

Figure 10. Time series of selected zonal ($m = 0$) coefficients from GRACE only and GPS/GRACE combination solutions. The GPS data augment the inaccurate solutions of GRACE's $C_{2,0}$ coefficient and other coefficients during GRACE's deep resonance periods (large blue spikes).

concurrently, the negative anomaly also moved west and appeared over Australia (from the sine component). In the middle of year, the positive anomaly appeared in the South Pacific Ocean and the negative anomaly in Europe. During the third quarter of year, the positive anomaly appeared in Australia and the negative anomaly in the North Atlantic Ocean. We hypothesize that this is the overall seasonal migration

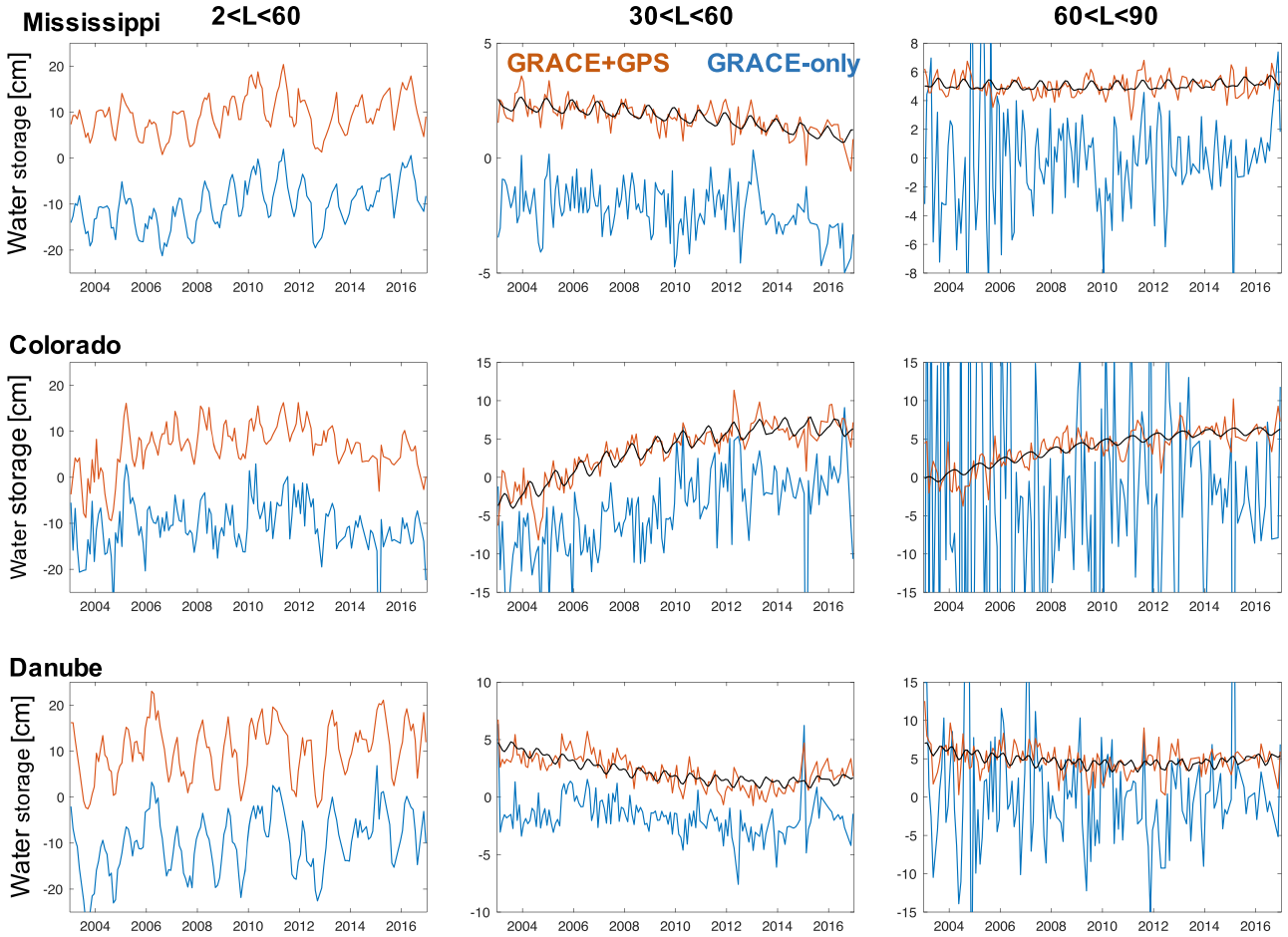

Figure 11. Terrestrial water storage changes estimated in three major river basins from GRACE only (blue) and GPS/GRACE joint inversion solutions (red). These river basins (Mississippi, Colorado, and Danube) are among the ones most effectively influenced by inclusion of GPS data with dense spatial coverage. The water storage time series was computed at three different degree bands (2–60, 30–60, and 60–90) to highlight the effect of GPS data at higher degrees. The water storage time series at the degree band of 30–90 are clearly improved by the GPS and GRACE combined solutions. The black curves represent the least-squares fit to the time series using the annual and semi-annual harmonic components and linear and quadratic parameters.

pattern of the degree-1 surface mass load of terrestrial water storage, atmosphere, and ocean masses, resulting in the seasonal geocenter motion. As seen from Figure 7, the Earth deforms responding to the migration of such degree-1 load. In the beginning of year, the United States, Africa, and Australia shift toward the positive load in Europe. Six months later, the horizontal motions of global GPS sites point to the degree-1 load in the South Pacific Ocean. The results from the SLR solutions are similar to those of our GPS/GRACE solutions.

The mass load from all other degrees ($l \geq 2$), which are what GRACE measures, is as large as a few decimeters in the Amazon, ~10 cm over the Eurasian and European continents, and only a few centimeters over the arid and semi-arid regions including Australia (Figure 12, bottom panel). Depending on the region, the contribution of the degree-1 mass load to the total mass changes could be as important as the contribution from all other higher degrees in arid basins. The accurate determination of the degree-1 load (causing the geocenter motion) is crucial to quantify total water mass changes particularly in arid areas.

Figure 13 illustrates the water storage changes in the Lake Eyre basin, Australia and the Nile river basin, Africa. The monthly time series from the degree-1 load and higher degrees from our GPS/GRACE inversion solutions are shown. Since we are interested in only land water storage in this example, the atmosphere and ocean component of the degree-1 load was computed separately using the degree-1 coefficients of the AOD

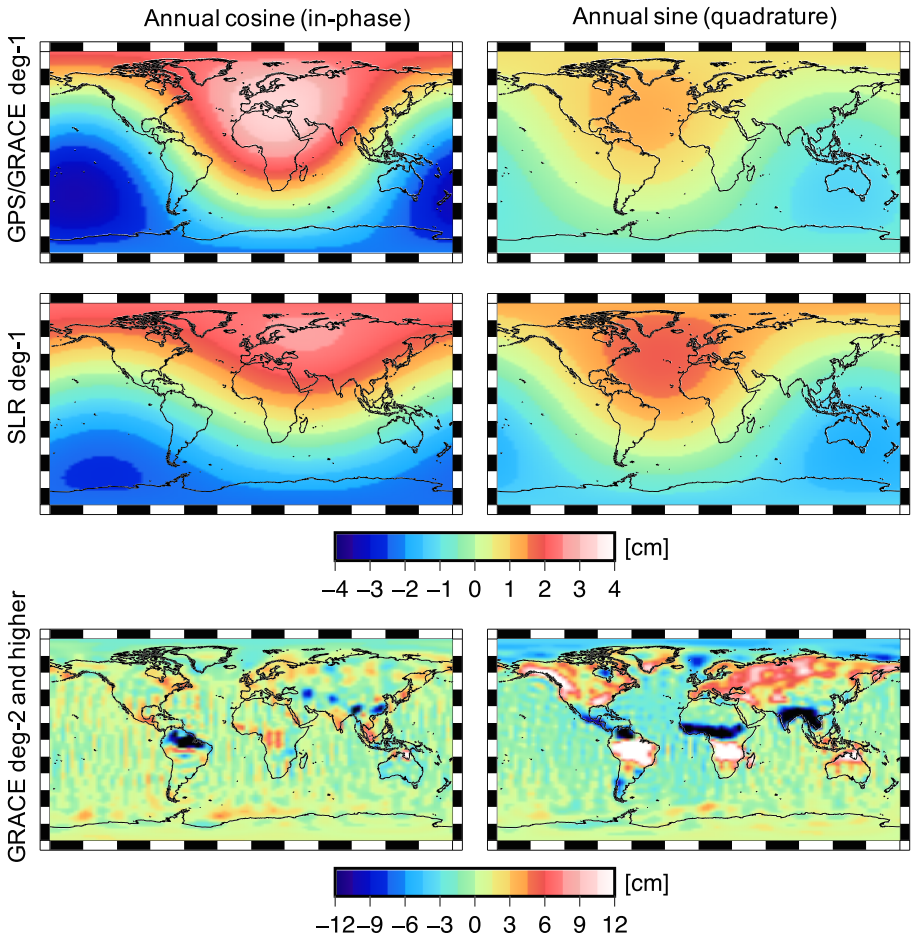

Figure 12. Spatial patterns of annual degree-1 surface mass load estimated from our (top panels) GPS/GRACE joint inversion and (middle panels) SLR solutions and of (bottom panels) seasonal mass load from GRACE geopotentials of $l \geq 2$. The surface mass load was evaluated in terms of equivalent water thickness. The annual changes were presented as the in-phase and quadrature components. Note the difference in the amplitude and extent of the contrasting degree-1 solutions. A specific example of a difference that would influence regional deformation results is for the "in-phase" plots for GPS/GRACE deg-1 and SLR deg-1 in southern Alaska (see contrasting deformation vectors in Figure 7a).

model and removed from our GPS/GRACE degree-1 solutions. In both river basins, the changes by the degree-1 load are as large as the signal contribution from all other degrees.

In the right panel, we compared different degree-1 solutions from SLR and S08 (again, the AOD degree-1 components were removed) with our GPS/GRACE solutions in these basins. In the Lake Eyre basin, our GPS/GRACE and SLR solutions of degree-1 contribution to land water storage shows the peak of 3 cm water load in August, while the other higher degrees present the peak water storage of 3 cm in March. The total terrestrial water storage should be a combination of both. The results from the S08 degree-1 solutions are smaller by 50% and the peak was delayed by one to two months relative to the GPS/GRACE and SLR solutions. In the Nile river basin, both GPS/GRACE and SLR solutions present the peak anomaly of 1–2 cm in January–December, while the storage from higher degrees show the peak of 6 cm in September–October. The results from the S08 solutions imply small changes, only ~5 mm, that is quite different from other solutions for this basin. The uncertainty in the degree-1 components is indeed an important error source of quantifying total water storage changes in these arid and semi-arid basins.

3.6. Effect of Heterogeneity of Earth's Elastic Structure

Our analysis presented so far assumes that the Earth's elastic response (in geopotential change and surface deformation) to surface mass load is known through an elastic Earth model used to compute the load Love

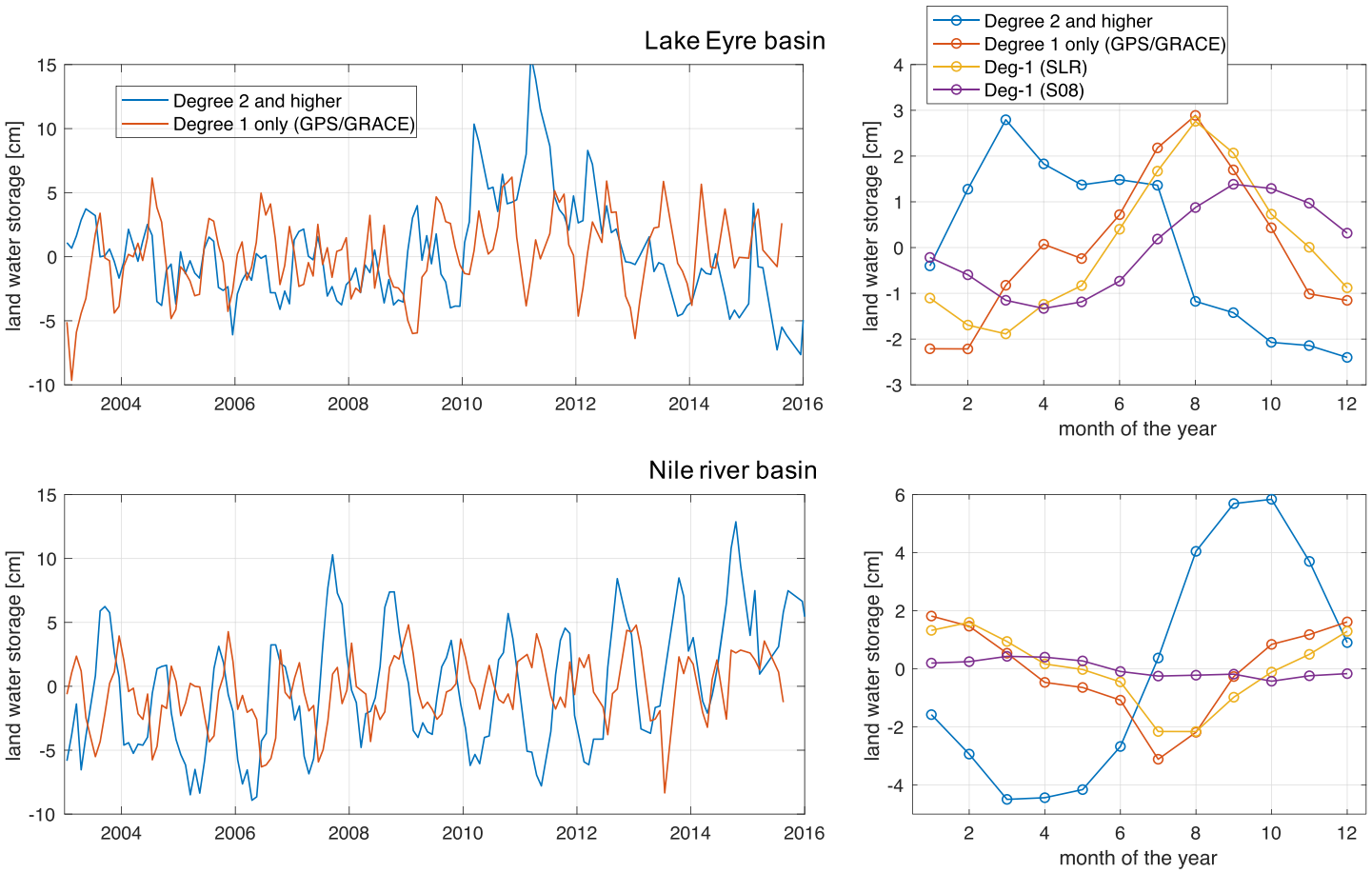

Figure 13. (left) Monthly time series of terrestrial water storage change in Lake Eyre (Australia) and Nile basins, computed from GRACE geopotential coefficients of $l \geq 2$ (blue), our GPS/GRACE degree-1 solutions (red) after removing the degree-1 components of atmosphere and ocean mass from the AOD model, to highlight land water effects only. In the Lake Eyre basin the large increase in water storage starting 2010 and the decrease from 2012 observed by GRACE corresponds to the La Niña in Australia. (right) The average monthly changes during 2003–2016 estimated from GRACE (blue) and our degree-1 solutions (red) and from SLR (yellow) and S08 (purple) degree-1 solutions (again, the AOD degree-1 removed from different degree-1 solutions). The degree-1 contribution to the total land water storage change could be as large as all other degrees in the Lake Eyre basin and ~40% of all other degrees in Nile river basin. The significant uncertainty among different degree-1 solutions highlights how important it is to obtain more accurate solutions for geocenter motion.

numbers in equations (2)–(5). We used the global average Earth structure of Preliminary Reference Earth Model (PREM) that defines the elastic parameters including density, shear modulus (rigidity), and bulk modulus at different depths. It is unambiguously observed that there are significant differences in the elastic structure in the lithosphere (top 300 km) and upper mantle across the contiguous United States (Bensen et al., 2009; Pasyanos et al., 2014; Shen & Ritzwoller, 2016). The seismic tomography for the U.S. continent found the dichotomy of shear wave velocity V_s within top ~300 km between the tectonically-active western United States (west of the Rocky Mountain front) and the eastern United States. The eastern region is characterized by a thicker lithosphere (~300 km) and higher V_s (~10%) than the lithosphere and velocity of the western United States (Pasyanos et al., 2014; Shen & Ritzwoller, 2016). The higher V_s means larger rigidity μ and/or lower density ρ through $V_s = \sqrt{\mu/\rho}$, and leads to smaller deformation for a given load. The change in rigidity yields greater change in vertical load deformation than in horizontal deformation, as shown analytically in equations (13) and (15) of Farrell (1972). The question is if such change in the elastic properties across the North American continent in the United States may yield a change in load deformation detectable by GPS. The difference in elastic properties may complicate the use of GPS and GRACE measurements for recovering surface mass load.

We computed different sets of the load Love numbers by perturbing density, rigidity, and bulk modulus within the lithosphere according to different profiles of seismic wave velocities from LITHO1.0 model (Pasyanos et al., 2014). We found that the lithosphere thickness changes within 50 to 300 km in the western to eastern United States. In the eastern United States, the shear wave is faster up to 10% and density is lower by a few percent compared to PREM. These departures form PREM yield a rigidity increase by up to 20%. This translates into up to 6% of smaller vertical deformation and little change in lateral displacement and geopotential at the maximum degree and order of 90. In the contiguous United States, the largest annual vertical displacement is found to be around 10 mm. The change caused by the lateral variation of the elastic properties in the lithosphere is likely to be a secondary effect, considering the GPS positional accuracy at present.

4. Summary and Conclusion

GRACE gravitational potential data are being used in numerous applications for studying mass redistribution on the Earth's surface. The data have been analyzed in conjunction with geophysical models and other geodetic data including GPS measurements of surface deformation. Unlike other models and data sets made available in a more intuitive reference frame attached to the Earth's surface, GRACE data are referenced to the frame located at the center of mass of the Earth system (geocenter). The geocenter moves within a few millimeters in all three axes from its long-term mean position due to seasonal migration of atmospheric, oceanic, terrestrial water, and ice/snow masses. Such subtle translation between the reference frames must be accounted for when GRACE data are used to quantify surface mass changes. The global network of GPS stations has been measuring 3D surface displacement as a result of the solid Earth's deformation to surface mass load. The GPS data can be used to determine the surface mass redistribution independently from GRACE. Unlike GRACE data, GPS displacement data are referenced to a frame like ITRF.

In this paper, we developed and demonstrated a method to jointly invert GPS displacement data and GRACE geopotential data to determine global geopotential fields in a consistent ITRF reference frame. All geopotential coefficients were estimated simultaneously and seamlessly from degree-1. New solutions of geocenter motion and geopotential field were determined by analyzing daily position solutions from 1,651 GPS stations and monthly GRACE data from 2003 to 2016.

We found the horizontal GPS displacement data to be particularly sensitive to the degree-1 surface mass load as a result of geocenter motion, as also shown by Han (2016) and Chanard et al. (2018). We found that it is possible to estimate the geocenter motion only from horizontal GPS displacement data along with GRACE data. In the United States, the X and Y components of the geocenter motion can be readily seen from east and north GPS displacement data, respectively, even without any data processing. The United States moves northwest in the beginning of year and southwest in the middle of year in response to the seasonal migration of the degree-1 mass load. Our geocenter motion solutions agreed best with the SLR solutions within 1 mm in the X and Z components and submillimeter in the Y component when compared in monthly variability averaged over 2003–2016. Indeed, various geocenter motion solutions agreed best in the Y component. However, our GPS/GRACE geocenter solutions are contaminated by systematic error associated with GPS data at the draconitic period and its overtones. The use of GPS horizontal time series (after detrending to compensate for plate motion) makes it difficult to determine a secular drift in the geocenter motion.

The vertical GPS displacement data from a dense GPS network are useful for improving the geopotential field at higher degrees and orders. We demonstrated that the geopotential fields become more systematic by virtue of including GPS data in our solutions and this is most evident in higher-order ($m \geq 16$) coefficients. The GPS data also corrected the noisy higher-degree zonal ($m = 0$) coefficients of GRACE geopotential solutions. Also, we illustrated improved water storage estimates from higher degrees ($l \geq 20$) for the U.S. and European river basins where dense GPS network are available.

The accurate determination of geocenter motion is critical to quantifying GRACE water storage particularly in arid and semi-arid areas as well as ocean mass recovery from GRACE and altimeter data (e.g., Chambers et al., 2007). For example, in the Lake Eyre basin, Australia, the present geocenter motion solutions from different techniques differ by 2 cm in equivalent water height with a phase difference of a couple of months, while total water storage is only about 3 cm in annual change. The uncertainty of geocenter motion is a significant error source in quantifying terrestrial water storage change in the Australian basin.

The geocenter motion solution from our GPS/GRACE joint analysis is contaminated by the systematic error in GPS geocentric positional data at draconitic period and its overtones, particularly in the horizontal data. If these time series become long enough, the solutions can be improved by filtering out over the draconitic period. The GPS/GRACE joint inversion approach can be further enhanced by (1) explicitly parameterizing the draconitic harmonic terms that are geographically-correlated to remove them from GPS data, (2) considering the full covariance matrix among different GPS stations, (3) estimating GPS orbital parameters simultaneously with geopotential fields from more fundamental GPS data like SINEX files (Blewitt, 1998), (4) more carefully pre-screening GPS sites that present local changes less coherent with regional deformation. A priori spatial filtering (like kriging) of GPS data could be useful in this regard, and, finally, (5) parameterizing poroelastic deformation which behaves in the opposite sense to elastic load deformation with time delay (e.g., Bawden et al., 2001; Wisely & Schmidt, 2010). Lastly, the effect of inhomogeneous GPS network distribution (heavily on United States and Europe) on the geocenter motion solutions needs to be examined.

Acknowledgments
This work is funded by The University of Newcastle to support NASA's GRACE and GRACE Follow-On projects as an international science team member to the missions and by Australian Research Council (DP170100224) as well as NASA support to J. Sauber as a science team member. We thank DLR for GRACE telemetry data and JPL, CSR, and GFZ for the high-quality Level-1B and Level-2 data. The GRACE data and AOD models were obtained from the website *GRACE Tellus* (https://grace.jpl.nasa.gov). GPS data were downloaded from https://sideshow.jpl.nasa.gov/post/series.html. SLR data and S08 solutions were available from https://grace.jpl.nasa.gov/data/get-data/geocenter/. The authors thank Xiaoping Wu (JPL) for his degree-1 solutions from the global inverse approach. Don Chambers, an anonymous reviewer, and an Associate Editor provided constructive reviews which were used to substantially improve the original results and manuscript.

References

Altamimi, Z., Rebischung, P., Métivier, L., & Xavier, C. (2016). ITRF2014: A new release of the International Terrestrial Reference Frame modeling nonlinear station motions. *Journal of Geophysical Research: Solid Earth*, *121*, 6109–6131. https://doi.org/10.1002/2016JB013098

Argus, D. F., Landerer, F. W., Wiese, D. N., Martens, H. R., Fu, Y., Famiglietti, J. S., et al. (2017). Sustained water loss in California's mountain ranges during severe drought from 2012 to 2015 inferred from GPS. *Journal of Geophysical Research: Solid Earth*, *122*, 10,559–10,585. https://doi.org/10.1002/2017JB014424

Bawden, G. W., Thatcher, W., Stein, R. S., Hudnut, K. W., & Peltzer, G. (2001). Tectonic contraction across Los Angeles after removal of groundwater pumping effects. *Nature*, *412*(6849), 812–815. https://doi.org/10.1038/35090558

Bensen, G. D., Ritzwoller, M. H., & Yang, Y. (2009). A 3D shear velocity model of the crust and uppermost mantle beneath the United States from ambient seismic noise. *Geophysical Journal International*, *177*(3), 1177–1196.

Bettadpur, S. (2012). UTCSR Level-2 Processing Standards Document, Rev 4.0 May 29, 2012.

Blewitt, G. (1998). GPS data processing methodology: From theory to applications. In P. J. G. Teunissen, & A. Kleusberg (Eds.), *GPS for Geodesy* (pp. 231–270). New York: Springer.

Blewitt, G., & Clarke, P. (2003). Inversion of Earth's changing shape to weigh sea level in static equilibrium with surface mass redistribution. *Journal of Geophysical Research*, *108*(B6), 2311. https://doi.org/10.1029/2002JB002290

Blewitt, G., Hammond, W. C., & Kreemer, C. (2018). Harnessing the GPS data explosion for interdisciplinary science. *Eos*, *99*. https://doi.org/10.1029/2018EO104623

Blewitt, G., Lavallee, D., Clarke, P., & Nurutdinov, K. (2001). A new global mode of Earth deformation: Seasonal cycle detected. *Science*, *294*, 2342–2345.

Borsa, A. A., Agnew, D. C., & Cayan, D. R. (2014). Ongoing drought-induced uplift in the western United States. *Science*, *345*(6204), 1587–1590. https://doi.org/10.1126/science.1260279

Caron, L., Ivins, E. R., Larour, E., Adhikari, S., Nilsson, J., & Blewitt, G. (2018). GIA model statistics for GRACE hydrology, cryosphere, and ocean science. *Geophysical Research Letters*, *45*, 2203–2212. https://doi.org/10.1002/2017GL076644

Chambers, D., Tamisiea, M., Nerem, R. S., & Ries, J. (2007). Effects of ice melting on GRACE observations of ocean mass trends. *Geophysical Research Letters*, *34*, L05610. https://doi.org/10.1029/2006GL029171

Chambers, D. P., Wahr, J., Tamisiea, M. E., & Nerem, R. S. (2010). Ocean mass from GRACE and glacial isostatic adjustment. *Journal of Geophysical Research*, *115*, B11415. https://doi.org/10.1029/2010JB007530

Chanard, K., Fleitout, L., Calais, E., Rebischung, P., & Avouac, J.-P. (2018). Toward a global horizontal and vertical elastic load deformation model derived from GRACE and GNSS station position time series. *Journal of Geophysical Research: Solid Earth*, *123*, 3225–3237. https://doi.org/10.1002/2017JB015245

Chao, B. F. (2016). Caveats on the equivalent water thickness and surface mascon solutions derived from the GRACE satellite-observed time-variable gravity. *Journal of Geodesy*, *90*(9), 807–813. https://doi.org/10.1007/s00190-016-0912-y

Cheng, M. K., Ries, J. C., & Tapley, B. D. (2013). Geocenter Variations from Analysis of SLR data. In *Reference Frames for Applications in Geosciences, International Association of Geodesy Symposia* (Vol. 138, pp. 19–26). Berlin Heidelberg: Springer-Verlag.

Clarke, P. J., Lavallée, D. A., Blewitt, G., van Dam, T. M., & Wahr, J. M. (2005). Effect of gravitational consistency and mass conservation on seasonal surface mass loading models. *Geophysical Research Letters*, *32*, L08306. https://doi.org/10.1029/2005GL022441

Dobslaw, H., Flechtner, F., Bergmann-Wolf, I., Dahle, C., Dill, R., Esselborn, S., et al. (2013). Simulating high-frequency atmosphere-ocean mass variability for dealiasing of satellite gravity observations: AOD1B RL05. *Journal of Geophysical Research: Solid Earth*, *118*, 3704–3711. https://doi.org/10.1002/jgrc.20271

Farrell, W. E. (1972). Deformation of the Earth by surface loads. *Reviews of Geophysics*, *10*, 761–797. https://doi.org/10.1029/RG010i003p00761

Fu, Y., Argus, D. F., & Landerer, F. W. (2015). GPS as an independent measurement to estimate terrestrial water storage variations in Washington and Oregon. *Journal of Geophysical Research: Solid Earth*, *120*, 552–566. https://doi.org/10.1002/2014JB011415

Griffiths, J., & Ray, J. R. (2013). Sub-daily alias and draconitic errors in the IGS orbits. *GPS Solutions*, *17*, 413–422.

Han, S.-C. (2016). Seasonal clockwise gyration and tilt of the Australian continent chasing the center of mass of the Earth's system from GPS and GRACE. *Journal of Geophysical Research: Solid Earth*, *121*, 7666–7680. https://doi.org/10.1002/2016JB013388

Han, S.-C., Broerse, T., Riva, R., Sauber, J. (2019). Reappraisal of the great earthquakes using GRACE measurements of gravitational field changes and development of earthquake gravity correction models, a paper presented at 27th International Union of Geodesy and Geophysics, Montreal, Canada, July 8-18, 2019.

Han, S.-C., & Razeghi, S. M. (2017). GPS recovery of daily hydrologic and atmospheric mass variation: A methodology and results from the Australian continent. *Journal of Geophysical Research: Solid Earth*, *122*, 9328–9343. https://doi.org/10.1002/2017JB014603

Han, S.-C., Riva, R., Sauber, J., & Okal, E. (2013). Source parameter inversion for recent great earthquakes from a decade-long observation of global gravity fields. *Journal of Geophysical Research: Solid Earth*, *118*, 1240–1267. https://doi.org/10.1002/jgrb.50116

Heflin, M., Moore, A., Murphy, D., Desai, S., Bertiger, W., Haines, B., et al. (2018). Introduction to JPL's GPS Time Series, https://sideshow.jpl.nasa.gov/post/tables/GPS_Time_Series.pdf

Heiskanen, W. A., & Moritz, H. (1967). *Physical Geodesy*. San Francisco, Calif: W. H. Freeman.

Jekeli, C. (2015). In G. Schubert (Ed.), *Potential Theory and the Static Gravity Field of the Earth*, *Treatise on Geophys* (2nd ed., Vol. 3, pp. 9–35). Oxford: Elsevier.

Koch, K.-R. (1999). *Parameter Estimation and Hypothesis Testing in Linear Models*. New York: Springer.

Kusche, J., & Schrama, E. J. O. (2005). Surface mass redistribution inversion from global GPS deformation and Gravity Recovery and Climate Experiment (GRACE) gravity data. *Journal of Geophysical Research*, *110*, B09409. https://doi.org/10.1029/2004JB003556

Lavallée, D. A., van Dam, T., Blewitt, G., & Clarke, P. J. (2006). Geocenter motions from GPS: A unified observation model. *Journal of Geophysical Research*, *111*, B05405. https://doi.org/10.1029/2005JB003784

Mayer-Gürr, T., Behzadpour, S., Ellmer, M., Kvas, A., Klinger, B., Zehentner, N. (2016). ITSG-Grace2016 - Monthly and Daily Gravity Field Solutions from GRACE. GFZ Data Services. http://doi.org/10.5880/icgem.2016.007

Pasyanos, M. E., Masters, T. G., Laske, G., & Ma, Z. (2014). LITHO1.0: An updated crust and lithospheric model of the Earth. *Journal of Geophysical Research: Solid Earth*, *119*, 2153–2173. https://doi.org/10.1002/2013JB010626

Petit, G., & Luzum, B. (2010). In G. Petit, & B. Luzum (Eds.), *IERS Conventions (2010), IERS Technical Note* (Vol. 36, p. 179). Frankfurt am Main: Verlag des Bundesamts für Kartographie und Geodäsie.

Ray, J., Altamimi, Z., Collieux, X., & van Dam, T. (2008). Anomalous harmonics in the spectra of GPS position estimates. *GPS Solutions*, *12*, 55–64. https://doi.org/10.1007/s10291-007-0067-7

Rodriguez-Solano, C. J., Hugentobler, U., Steigenberger, P., Bloßfeld, M., & Fritsche, A. (2014). Reducing the draconitic errors in GNSS geodetic products. *Journal of Geodesy*, *88*(6), 559–574. https://doi.org/10.1007/s00190-014-0704-1

Shen, W., & Ritzwoller, M. H. (2016). Crustal and uppermost mantle structure beneath the United States. *Journal of Geophysical Research: Solid Earth*, *121*, 4306–4342. https://doi.org/10.1002/2016JB012887

Sun, Y., Riva, R., & Ditmar, P. (2016). Optimizing estimates of annual variations and trends in geocenter motion and J2 from a combination of GRACE data and geophysical models. *Journal of Geophysical Research: Solid Earth*, *121*, 8352–8370. https://doi.org/10.1002/2016JB013073

Swenson, S., Chambers, D., & Wahr, J. (2008). Estimating geocenter variations from a combination of GRACE and ocean model output. *Journal of Geophysical Research*, *113*, B08410. https://doi.org/10.1029/2007JB005338

Tapley, B. D., Bettadpur, S., Watkins, M., & Reigber, C. (2004). The gravity recovery and climate experiment: Mission overview and early results. *Geophysical Research Letters*, *31*, L09607. https://doi.org/10.1029/2004GL019920

Tapley, B. D., Watkins, M. M., Flechtner, F., Reigber, C., Bettadpur, S., Rodell, M., et al. (2019). Contributions of GRACE to understanding climate change. *Nature Climate Change*, *9*(5), 358–369. https://doi.org/10.1038/s41558-019-0456-2

Wahr, J., Molenaar, M., & Bryan, F. (1998). Time variability of the Earth's gravity field: Hydrological and oceanic effects and their possible detection using GRACE. *Journal of Geophysical Research*, *103*, 30,205–30,229. https://doi.org/10.1029/98JB02844

Webb et al. (2018). GRACE-FO Mission Status and Further Plans, a paper presented at GRACE/GRACE-FO Science Team Meeting, Helmholtz Centre Potsdam - GFZ German Research Centre for Geosciences, 9-11 October 2018

Wisely, B. A., & Schmidt, D. (2010). Deciphering vertical deformation and poroelastic parameters in a tectonically active fault-bound aquifer using insar and well level data, san bernardino basin, california. *Geophysical Journal International*, *181*(3), 1185–1200. https://doi.org/10.1111/j.1365-246X.2010.04568.x

Wolf, H. (1977). Zur Grundlegung der Kollokationsmethode. *Zeitschrift für Vermessungswesen*, *102*(6), 237–239.

Wu, X., Heflin, M. B., Schotman, H., Vermeersen, B. L. A., Dong, D., Gross, R. S., et al. (2010). Simultaneous estimation of global present-day water transport and glacial isostatic adjustment. *Nature Geoscience*, *3*(9), 642–646. https://doi.org/10.1038/ngeo938

Wu, X., Ray, J., & van Dam, T. (2012). Geocenter motion and its geodetic and geophysical implications. *Journal of Geodynamics*, *58*, 44–61.